8

Fractal Analysis of Scaling and Spatial Clustering of Fractures

C. C. Barton

8.1. INTRODUCTION

Fractures exist over a wide range of scales, from the largest faults to microfractures, and this range is primarily responsible for scaling effects observed in fractured-rock hydrology and bulk mechanical properties of fractured rock (Witherspoon and others, 1979; Thorp and others, 1983; DeMarsily, 1985).

Fractal geometry is a branch of mathematics that can identify and quantify how the geometry of patterns repeats from one size to another. The repetition of fracture patterns over a wide range of scales is qualitatively demonstrated by the need to place an object of known size, such as a coin, hammer, or person, into photographs or a scale bar on photomicrographs and maps to establish scale. This is illustrated in Fig. 8.1, which shows a series of photographs of fracture patterns whose scales, rock types, ages, and deformation histories are different. Figure 8.1 also illustrates that fracture patterns can range from ordered (8.1d) to disordered (8.1a–c). Fractal geometry provides a method for quantifying the size scaling and spatial clustering of the full range of complexity found in networks of fractures. Fractal geometry also provides a means for extrapolating fracture properties from topologically limited samples, such as boreholes, which are one-dimensional samples, to three-dimensional fracture networks. Finally fractal geometry can be used to determine or constrain size scaling and spatial clustering of synthetic computer-generated fracture networks.

Quantitative understanding of size scaling and spatial clustering is fundamental to a quantitative understanding of fractured-rock hydrology and the bulk mechanical properties of fractured rock. This is because fluid flow and mechanical deformation do not use fractures at any one size scale but integrate the contribution of fractures at all scales, from

C. C. Barton • US Geological Survey, MS 940, Denver, Colorado.

Fractals in the Earth Sciences, edited by Christopher C. Barton and Paul R. La Pointe, Plenum Press, New York, 1995.

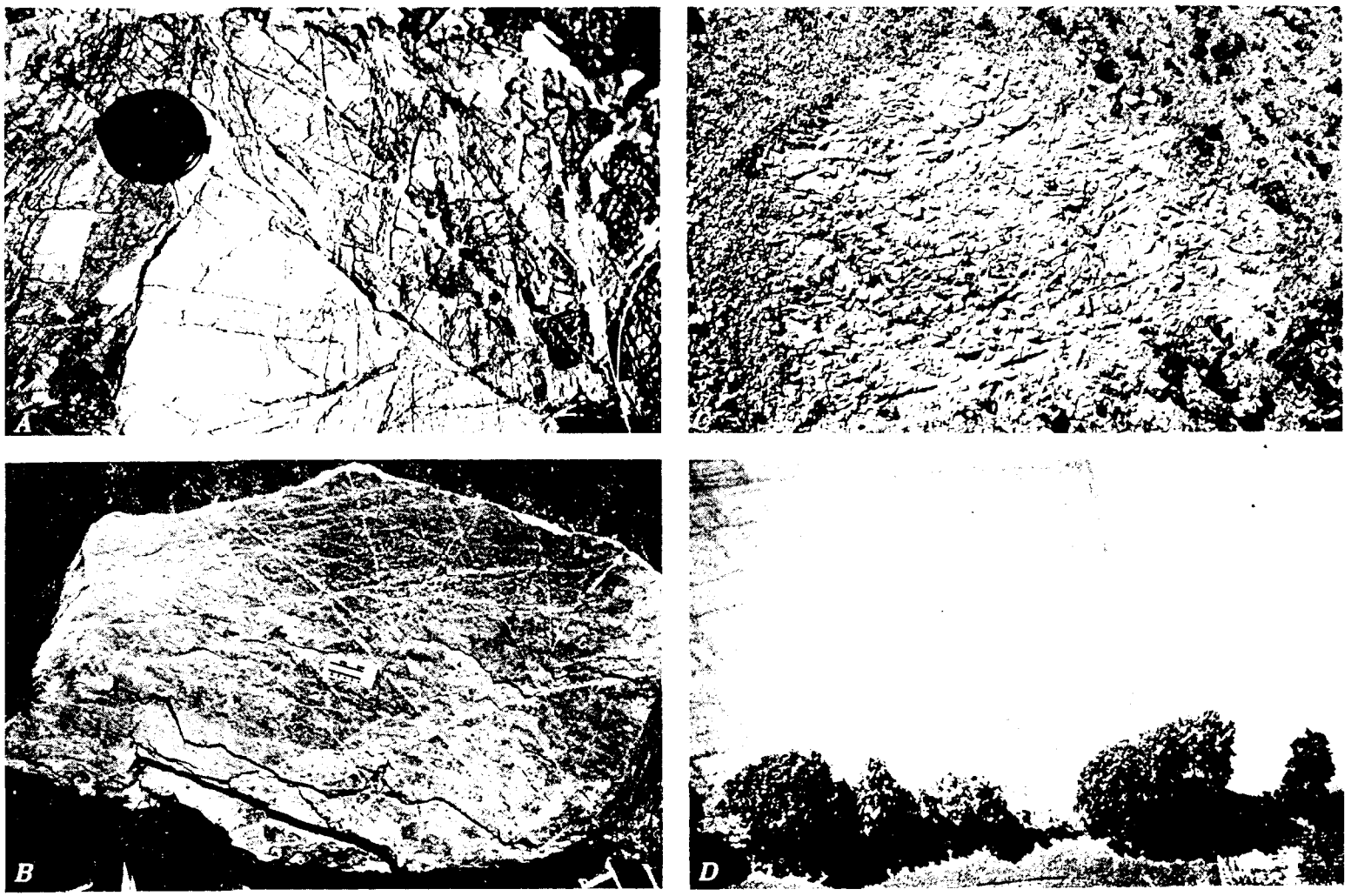

FIGURE 8.1. Photographs of fracture patterns at different scales. (a) Volcanic tuff, Calico Hills, NV; lens cap is 5 cm in diameter. (b) Sandstone, Morrison, CO; scale bar is 10 cm long. (c) Volcanic tuff, Yucca Mountain, NV; arrow is 2 m long. (d) Dolomite, Sturgeon Bay, WI; trees are approximately 12 m high. Fracture traces in (d) are outlined by alfalfa plants drawing water and nutrients from bedrock fractures underlying 0.3 m of soil. (Photo courtesy of Kenneth Bradbury.)

microfractures to the largest scale of interest. While there is a power law increase in the abundance of fractures as we move to smaller sizes (Barton and Hsieh, 1989), the contribution of smaller and smaller fractures to fluid flow and bulk mechanical deformation depends on the geometry of fracture connections within the network (Barton and Scholz, in press). For fluid flow, we must also consider the parameter of fracture volume (aperture times length times width), which must be finite for any given volume of rock. When the geometry of connectivity is convergent, even though there is a power law increase in the number of smaller fractures, the contribution of fractures of smaller sizes is correspondingly less important. Fractal behavior of trace length tells us how to scale the fractures of smaller sizes, but not the relative contribution of the fracture-trace length to flow. For flow-through fractures interconnected in parallel networks (in contrast to series networks), the largest fractures contribute most, and the effect of fractures at sizes less than one to two orders of magnitude less than the scale of the problem are minimal. In natural systems, the lower size limit may be reached even before the convergence limit. For fluid flow through rock, there is a transition at the size scale of the pores below which scale the fracture flow problem reduces to that of flow through a porous media whose pattern of flow has been shown to be fractal (see Oxaal and others, 1987). Fractal behavior of fractures also provides a basis for extrapolation in size from the scale of fracture data collection.

The concept of a representative elementary volume (REV) of rock was introduced by Bear (1972) as a means of characterizing and extrapolating hydrologic properties of porous media. Because the largest pore size is usually limited to a few millimeters in most rock types, a representative elementary volume need be only some small multiple of the pore size. Extending the REV concept to fractured rocks has been suggested by Long and others (1985) but it is problematic because there is no characteristic size limit to fractures. Moreover the REV concept assumes linear scaling, while fracture networks exhibit fractal (power law) scaling. Because fracture networks are fractal, the concept of characterizing a small part and extrapolating to the scale(s) of interest is possible, but not in the linear manner of the REV concept.

Connectedness within a fracture network is particularly important to the fluid flow properties of the network. Scaling and spatial-clustering distributions of connectedness lead to patches of high and low conductivity. Dead-end fractures contribute to the fluid storage capacity of the network, but not to flow across the network. Crossing and abutting intersections permit fracture segments in between to participate in flow across the network. In an attempt to quantify scaling and spatial-clustering patterns of interconnected segments in fracture networks, scaling and spatial-clustering distributions of crossing and abutting intersections should be analyzed.

Scales for the study of intermediate-sized fractures occurring as natural outcrops and roadcuts range from approximately 0.5–200 m in length. Until recently the study of rock fractures over this range has focused primarily on measuring the orientation of the fracture planes (for a summary, see Barton and Hsieh, 1989). Orientation frequency is normally plotted on rose diagrams (strike azimuth only) or stereographic projections (strike and dip), and it often reveals higher frequencies in one or more orientations that define what are termed fracture sets. Fractures not included in the set(s) are usually dropped from further analysis and interpretation. Alternatively some advocate a biased sampling procedure whereby the geologist visually judges what fracture set(s) are present in an outcrop, then records the orientation of only those fractures.

Interpreting fracture history; the relation of fractures to folds, large faults, and other

major tectonic features and fabrics; *in situ*- and paleo-principal stresses; the direction of fluid flow through fracture networks; and mechanical properties of fractured rock are defined traditionally in terms of fracture sets. Grouping fractures in sets defined by orientation frequency suppresses the heterogeneity of a complex system. The reduction of complex fracture patterns to highly ordered patterns has been practiced because the existing mathematics could best deal with highly ordered patterns. Ordered fracture patterns are normally found where only one or two generations of fractures are present except where mineralization has healed early generations. Fractal geometry is a mathematics especially well-suited to quantifying and modeling highly complex as well as ordered patterns.

A complete sampling of all fractures within some designated range of length or aperture is necessary to provide a representative sample for fractal analysis. Unfortunately most published geologic maps do not provide a representative sample of faults and other fractures either because of incomplete exposure and/or because no consistent criteria were used to show, not show, or interpolate fault traces. Often unstated criteria established during mapping are inconsistently applied to different rock types on the same map. Thus most published fault maps are too highly censored to permit a meaningful fractal analysis of spatial clustering and scaling of faults.

Chapter 8 touches a broad range of issues inherent in the study of scaling and spatial clustering of fractures, including one-, two-, and three-dimensional sampling of fracture networks, a review of fractal and nonfractal approaches for mathematically analyzing scaling and spatial clustering of fracture data sets, an introduction to the fractal box methods of measuring fracture data sets, and my own approaches for generating synthetic one- and two-dimensional models of fracture spacing and networks. A method of dissecting a fracture network into age generations (based on abutting relations) is presented, and this is the basis for explaining the transition from ordered to disordered fracture patterns; it is also the basis for generating synthetic fractal fracture networks. Comments on the implications of fractal behavior for the evolution of fracture networks are integrated throughout Chapter 8.

8.2. SAMPLING SPATIAL CLUSTERING AND SCALING OF FRACTURES IN ROCK

The methods of sampling spatial clustering and scaling of fractures in rock can be one-, two-, or three-dimensional. One-dimensional sampling is based on measuring the spacing between fractures along traverses across surface exposures or in boreholes in the subsurface. Two-dimensional sampling is based on mapping fracture traces exposed on subplanar exposures. Three-dimensional sampling requires geophysical imaging and mapping of fracture surfaces in a volume of rock. To my knowledge, there are no published studies of three-dimensional fracture networks detailed enough to permit quantitative analysis of their spatial and scaling properties. At present geophysical-imaging methods do not have the resolution necessary to image fractures adequately over the range of scales (one order of magnitude or more) required for fractal analysis, although the future is promising (Ramirez and Daily, 1987; Majer and others, 1988). A three-dimensional sample could be constructed by interpolating between closely spaced one-dimensional samples or between a sequence of parallel, closely spaced two-dimensional fracture trace maps. Such interpolation is commonly done for large faults, but usually sampling distance is too large to allow interpolation of the smaller fractures discussed in Chapter 8. Measuring the scaling of

fracture networks requires mapping fractures over a wide range of size scales. Optimally all sizes sampled can be shown on a single map: usually however as in Chapter 8, a series of maps is used, with each map sampling a range of size scale.

8.3. FRACTAL MEASURE OF SPATIAL AND SCALING PROPERTIES

Fractal geometry is a branch of mathematics that provides methods for quantifying the spatial and scaling properties of geometric data sets that are uncorrelated, positively correlated (persistent), or negatively correlated (antipersistent) as a function of scale or spatial distribution. Feder (1988) describes persistence and antipersistence. Persistence means that an increasing trend in preceding increments implies an increase in the next increment; conversely a decreasing trend in preceding increments implies a decrease in the next increment. Antipersistence means that an increasing trend in preceding increments implies a decreasing trend in the next and vice versa. In terms of fracture spacing, increasing persistence means increased clumping, and antipersistence leads to an even spacing. Fractal geometry is particularly well-suited to both positively and negatively correlated data sets. By comparison geostatistics (Journel and Huijbregts, 1978; Hohn, 1988) are applicable only to positively correlated data sets. Fractal patterns can be highly ordered or disordered, and this can be understood in terms of the procedures for generating fractal patterns, as described in the discussion of Cantor dusts. Fractal geometry also provides methods for creating synthetic analogs of natural geometries.

The geometry of a fractal pattern is represented by a fractional number, termed the fractal dimension (D). The size scale over which a fractal dimension applies is bounded by an upper and lower fractal limit. Fractal methods for analyzing spatial and scaling properties of objects are applicable to one-, two-, three-, or n-dimensional data sets.

8.4. METHODS OF MEASURING THE FRACTAL DIMENSION OF FRACTURE NETWORKS

8.4.1. Box Method

The box method is used in Chapter 8 to measure the fractal dimension of the spatial and scaling distribution of fractures. The method is robust in that it is applicable to self-similar and with certain restrictions, to self-affine data sets (see Chap. 4). The method is applicable to one- and two-dimensional data sets. In principle the method is simple: A sequence of grids, each with a different cell size, is placed over maps of fracture traces, then the number of cells intersected by fracture traces is counted. The fractal distribution is

$$Nr^{D} = 1 \tag{1a}$$

or equivalently

$$D = \frac{\log N}{\log (1/r)} \tag{1b}$$

where N is the number of cells containing portions of one or more fracture traces, r is the length of the side of the cell, and the fractal dimension D is the slope of straight-line segments fitted to the N, $1/r$ points plotted on logarithmic axes. A derivation of Eq. (1) is

given by Feder (1988) and by Pruess (Chap. 3). A schematic diagram of the counting procedure and the fractal plot are shown in Fig. 8.2.

Theoretically the fractal dimension is taken at the limit where the cell size goes to zero (Hausdorff, 1919) as discussed by Pruess (Chap. 3). This is not possible when analyzing real data sets with finite lower size limits. However, in Chapter 8 and my previous papers, the distribution of cell sizes is logarithmic, so there are progressively more smaller sized cells.

Fitting straight lines to points on the fractal plot is done using a least squares linear regression. Performing the regression in log-log space leads to a logarithmic weighting that favors smaller cell sizes. Breaks between lines of different slopes are located by visual inspection. Usually upper and lower fractal limits of data are exceeded by cell sizes that are too large and too small. These extra points are sequentially stripped off the ends of the plot until the slope of the line fit to the data stabilizes. This is a nonrigorous method that could be accomplished by such rigorous statistical method as jackknifing or bootstrapping, although the improvement would probably be minimal. The slope of the line is the fractal dimension, and the end points of the line are the upper and lower fractal limits. The least squares method of fitting a straight line to data permits calculating a goodness of fit by means of a correlation coefficient ranging from 0, for no correlation, to 1 for a perfect fit. I have tested the box method on fractal figures of known dimension (Koch curves) and found the error in dimension to be as great as 0.05. To improve the accuracy and reproducibility of the box method, I explored variations of the box method, as described in the following section.

8.4.2. Box-Rotate Method

In practice the procedure of overlaying grids is complicated by the need to overlay the grid so that for each cell size the minimum number of cells is occupied, a boundary condition stated by Hausdorff (1919) and incorporated into the derivation of Eq. 1. One way of accomplishing this is to rotate the grid relative to the data until for each cell size, the minimum number of cells is occupied. The effect of grid rotation on the fractal dimension

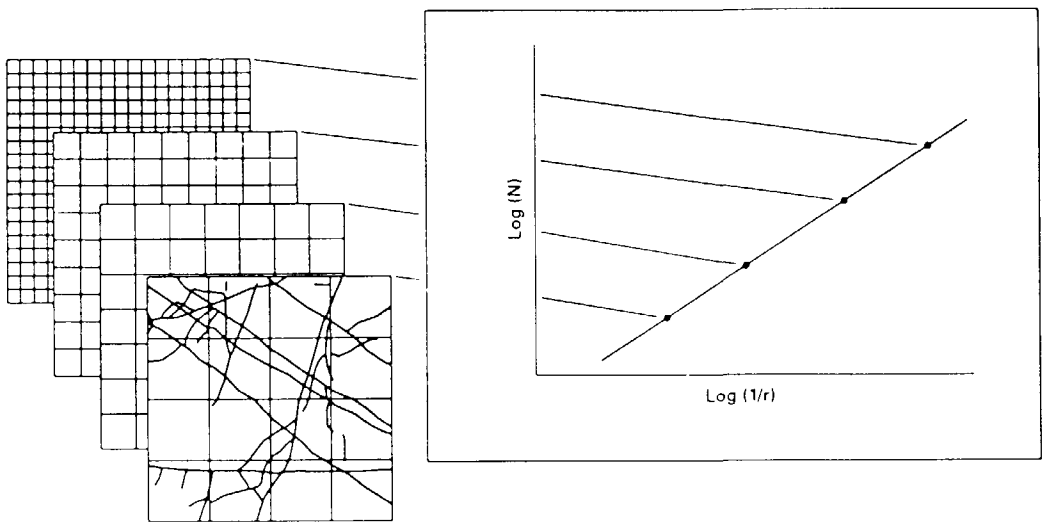

FIGURE 8.2. Illustration of the box method of measuring fractal dimension by overlaying a sequence of grids, each with a different cell size. For fractal data sets, a plot of the log of the number of occupied cells (N) versus the log of inverse cell size ($1/r$) yields data points that can be fit by a straight line whose slope is the fractal dimension (D), as stated in Eq. (1).

of a single straight line (whose true dimension is 1.000 . . . .) is shown in Fig. 8.3. Here the grid was rotated to the angle θ, and then the sequence of cells was counted. In Fig. 8.3, the increment of rotation angle θ is 2.5 degrees, and we can show analytically that for a single straight line, the minimum number of cells is occupied when θ equals 0, 45, or 90 degrees. At other orientations, additional cells are crossed; the number of such cells is given by the following equation:

$$N(r) = N_0(r) + \left[\frac{a}{r(\sin\theta)}\right] \tag{2}$$

Where $N(r)$ is the number of boxes crossed of size r, $N_0(r)$ is the number of boxes crossed of size r when $\theta = 0$, a is the length of the line (equal to 1 for unit length), and brackets [ ] indicate the integer part of the function within the brackets.

The consequence of not properly orienting the grid in the analysis of a straight line for each cell size is the introduction of an error of as much as 0.06 in the fractal dimension (Fig. 8.3). A single straight line is a worst case test because it is so highly anisotropic. Note that for complex shapes (Koch curves, for example), the equation is much more complicated than Eq. (2). Tests on Koch curves show that the error introduced when the grid is not oriented so that N is a minimum is as much as 0.05. When N is a minimum for each cell size, the error can still be as much as 0.02, because cells are squares that are not geometrically compatible with the Koch curve, whose angles are 60 and 120 degrees. Therefore for complex patterns, the box-rotate method is expected to have an error of approximately 0.02.

8.4.3. Box-Flex Method

Pruess (see Chap. 3) found that decreasing the increment between cell sizes so that tens, hundreds, or even thousands of cell sizes are used eliminates the need to orient grids properly. I tested Pruess's approach on shapes of known fractal dimension (Koch curves)

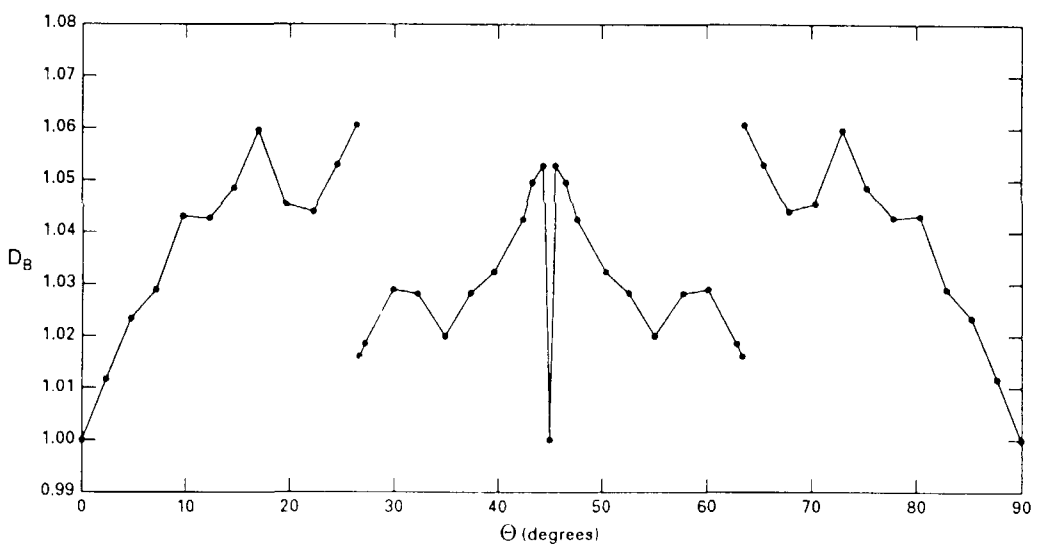

FIGURE 8.3. A plot of the variation in fractal dimension (D) for a straight line (whose dimension is 1) as a function of the orientation θ of the line measured in increments of 2.5 degrees. Note that the minimum number of cells, and therefore the true D, is occupied where $\theta = 0$, 45, and 90 degrees.

and found that the error was only 0.005 when using approximately 50 different cell sizes. To achieve small increments in cell size, it is necessary to allow the outer boundaries of the grid to expand and contract slightly because there must always be an integer number of boxes in the grid; there can be no fractional boxes. I term this the box-flex method and in Chapter 8, fractal dimensions are rounded up to the hundredth's decimal place.

8.4.4. Box-Density Method

In the box-counting methods just described, the size-scaling properties of a data set are measured by simply counting the number of occupied cells. La Pointe (1988) used a variation of the box method where the number of blocks bounded by fractures contained in each cell are counted. I call this the box-density method; it measures the spatial-clustering variation in a data set.

The procedure is to overlay a sequence of grids, then count the number of data points in each occupied cell. For each cell size, the maximum count is divided by the number of cells on one side of the grid. This value (Z) is then used to normalize the data such that for each cell in the grid, the sum of the normalized count is stored as N. The fractal dimension is calculated using Eq. (1) where N is this normalized value. A fractal dimension measured in this way ranges between 0–3.

8.5. PREVIOUS FRACTAL STUDIES OF THE SCALING AND SPATIAL DISTRIBUTION OF FRACTURES

Barton (1990), Velde and others (1990), Barton and Zoback (1992), and Manning (1994) reported fractal analyses of fracture spacing along a line sample. Barton (1990) reported on the spacing pattern of quartz/gold veins in cores from the Perseverance mine, which is described in detail later. Velde and others (1990) measured the fractal dimension in terms of a probability of finding a fracture-free zone in the following length unit to be measured. To study the effect of anisotropy in fracture patterns, researchers measured line samples at various orientations on two-dimensional fracture trace maps. The fractal dimension was observed to vary by as much as 0.33 for the most anisotropic of their fracture trace maps. The range of fractal dimension reported was 0.10–0.68. Visual observation of their fracture trace maps suggest that the very low fractal dimensions they obtained (all but four values less than 0.50) may be due to the sparseness of their data sets. Barton and Zoback (1992) fit the frequency of fracture-spacing intervals versus spacing interval from the Cajon Pass well, California, with a power law with a scaling exponent of 1.03. Note that their analysis of fracture spacing is different from that presented in Chapter 8 and other studies cited because they did not analyze a pattern of fractures with a box-counting procedure; rather they fit a spacing interval versus frequency plot with a power law. In such an analysis, the spatial sequence of fractures is lost, and results can not be compared with those reported elsewhere in Chapter 8. Manning (1994) reports on spacing metamorphic veins along linear transects in a variety of geologic settings. He finds the fractal dimension to range between 0.25–0.46 for sites in continental crust and to be 0.81 fo hydrothermally altered oceanic crust.

There have been several published fractal analyses of fracture trace maps. The first study was by Barton and Larsen (1985), who reported fractal dimensions for three fracture

patterns mapped at nearby locations in the same Miocene volcanic tuff unit at Yucca Mountain, Nevada. They used the box method and reported fractal dimensions ranging from 1.12–1.16. These values were calculated for cell sizes at and below the shortest fracture length and thus resulted in an improper analysis, unrepresentative of the fracture network. These same three patterns were reanalyzed using the box method over a wider range of cell sizes, which in part exceeded the size at which the fracture pattern was completely covered, by Barton and others (1986) along with four other fracture patterns and a fault map of the southern half of Yucca Mountain. Fractal dimensions of 1.5–1.9 were reported. The same three maps were reanalyzed by Barton and Hsieh (1989) using the box-rotate method in which again cell sizes in part exceeded the size at which the fracture pattern was completely covered, and fractal dimensions ranging from 1.6–1.7 were reported. I analyzed them yet again for this chapter, using the box-flex method over an appropriate range of box sizes, and I found the dimension ranges from 1.38–1.52. For the reasons stated in Section 8.4.3, the box-flex method provides the most accurate results.

Chiles (1988) used the box method to analyze fracture patterns mapped on drift walls in a granite mine. The drift walls were 2 m high and 50–100 m long. The minimum fracture trace length mapped was 0.2 m. Because of the limited height of the walls and a lower trace length cutoff at 0.2 m, the range of scales sampled vertically is considerably less than one order of magnitude. Examining the fractal plots in Chiles (1988) reveals that he permitted the cell size to be as small as 0.01 m, smaller than the smallest fracture trace (0.2 m) and thus improperly analyzed his maps in the same manner as Barton and Larsen (1985). A better range of box sizes for his maps would be 0.2–0.5 m rather than the 0.01–10 m he used. A fractal analysis of the spacing pattern of fractures along a line sample 50–100 m long (with the smallest cell size two times the shortest distance between two fractures and the largest cell size one-half the length of the longest distance between two fractures) would be a more appropriate way of analyzing data such sets as Chiles's.

La Pointe (1988) introduced the box-density method to the analysis of fracture trace maps. He counted the number of blocks bounded by fractures per cell rather than the number of fracture traces. He analyzed the three maps (reproduced in Figs. 8.7a–c) at Yucca Mountain published in Barton and Larsen (1985), a map (reproduced in Fig. 8.7i) from the Lannon area, Wisconsin, published in La Pointe and Hudson (1985), and several computer-generated synthetic maps. Instead of analyzing entire maps, he analyzed a strip taken as a representative subset of the map. His fractal dimensions for strips across the maps in Fig. 8.7a–c are 2.52, 2.37, and 2.69, respectively.

Hirata (1989) reported fractal dimensions for the pattern of seismogenic faults at various locations in Japan. He used the box method and reported fractal dimensions ranging from 0.72–1.60. Visual inspection of his maps reveals that those maps with fractal dimensions less than 1.5 contain very few fractures, and these are probably censored data sets when compared to the spatial density of fractures reported by King (1983) for seismogenic fault patterns. Also Hirata's fractal analyses include only five cell sizes. Based on my experience, the error in determining a fractal dimension using the box method with only five box sizes is large, as much as 0.15.

Korvin (1989) investigated the size distribution of fault-bounded blocks at the bottom of the southern end of the Gulf of Suez rather than scaling or spatial distributions of fractures traces. His plots of the cumulative frequency of block size can be interpreted as fractal. However because of the rollover at small block sizes and other changes in slope on some of his log-log plots, he interprets his plots as demonstrating nonfractal behavior.

Nonlinear behavior on a log-log plot does not necessarily mean that the data is nonfractal; the data may be scale variant or multifractal. I interpret the rollover he shows as due to data omission at smaller block sizes. His data can be fit with one or more straight-line segments whose slopes are the fractal dimension(s), although I have not done this.

8.6. ONE-DIMENSIONAL SAMPLING AND ANALYSIS OF FRACTURE NETWORKS

8.6.1. Sampling

Although fracture networks are three-dimensional, it is difficult or impossible to obtain a complete three-dimensional sample, as previously discussed. Boreholes, which provide one-dimensional samples of fracture networks, are the most frequently used method of sampling the spatial distribution of fractures in the subsurface. Straight-line, or scan-line traverses along surface outcrops are also one-dimensional samples. Both provide spacing from one fracture to the next. If orientation data are provided, then spacing between fractures of the same set can be studied (Barton, 1983), but this is not normally done. Methods of one-dimensional fracture sampling at the surface can be found in La Pointe and Hudson (1985) and Barton (1983). Methods of sampling subsurface fractures by direct observation in drill core are described in Kulander and others (1979) and by geophysical methods in drill holes in Paillet (1991).

8.6.2. Nonfractal Analysis Methods

There are a number of precedents to any study of scaling and spatial distributions of fractures in rock. Prior to the advent of fractal geometry, scaling and spatial properties were sampled, quantified, and modeled. However data collection was limited primarily to one-dimensional (linear) sampling of spacing between fractures intersected along a traverse, and mathematical treatments were for the most part limited to such linear samples. Few studies have measured the spacing-frequency for individual sets (Barton, 1983); most studies simply include all fractures encountered along the sample without regard for, or knowledge of, orientation, size, or other discriminator (for example, Priest and Hudson, 1976). In studies were fractures are grouped into sets based on orientation, the sampling interval consists of a traverse oriented perpendicular to fracture planes (Barton, 1983).

The mathematical analysis of spatial distribution in early papers was limited to calculating an arithmetic mean, and this approach persists to the present (summarized by Barton, 1983). In a series of papers, Priest and Hudson (1976, 1981), Baecher and others (1977), and Hudson and Priest (1979, 1983) treated frequency plots of fracture spacing as lognormal or negative exponential distributions. The cumulative probability plot for fracture spacing was introduced by Baecher and others (1977) and explored by Barton (1983) for two fracture sets in the same bed. Cumulative probability plots generate a mean and standard deviation, and like all other previous approaches, these simply plot the frequency of various spacing intervals without considering the sequence from one fracture to the next. La Pointe (1980) introduced and explored the use of semivariograms as a method for analyzing fracture spacing along a linear traverse (scan line). Semivariograms plot the second-order moment of the number of fractures per unit length of the scan line versus the length of the sampling

increment over some range of increment size analogous to cell size in the box method. Some semivariograms of spacing frequency reveal power law distributions where the power is a fraction rather than an integer. Such semivariogram plots can be recast into fractal plots by plotting the semivariance against sample increment size in log-log space and calculating the fractal dimension from the slope of straight line(s) fit to the points. The approaches just described are limited to spacing data collected along a line sample.

8.6.3. *Fractal Analysis of the Spatial Distribution of Quartz/Gold Veins in Exploratory Cores from the Perseverance Mine, Juneau, Alaska*

The spacing between gold-bearing quartz-filled fractures (veins) intersected by exploratory drilling from tunnels in the Perseverence mine provides a data set for analysis. Figure 8.4 shows a vertical cross section of the mine, the drilling pattern, and the location of quartz-filled fractures above a specified assay value along bore holes. Qualitatively the spacing has no discernible pattern or structure.

A fractal analysis was performed on the spacing distribution between veins on 23 cores, each approximately 90 m long and intersecting approximately 40–60 veins. The box-rotate method was used, with each drill hole rotated horizontally to minimize the number of occupied cells (see Section 8.4.2). A typical fractal plot of spacing is shown in Fig. 8.5, and the range of fractal dimensions is given in Table 8.1. The range in fractal dimension is 0.41–0.62, with goodness-of-fit coefficients greater than 0.98.

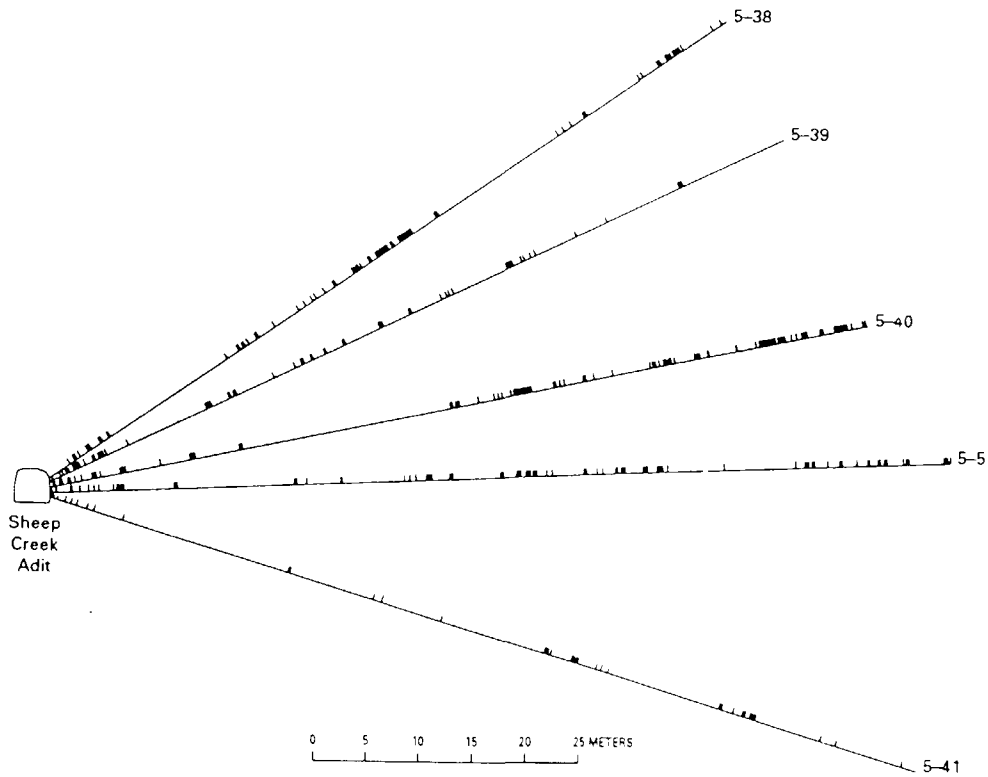

FIGURE 8.4. Vertical cross-section showing the fan pattern of core drilling from an adit in the Perseverence mine, Juneau, Alaska. The position and thickness of gold-bearing quartz veins filling fractures along each drill hole are shown by tick marks of appropriate width.

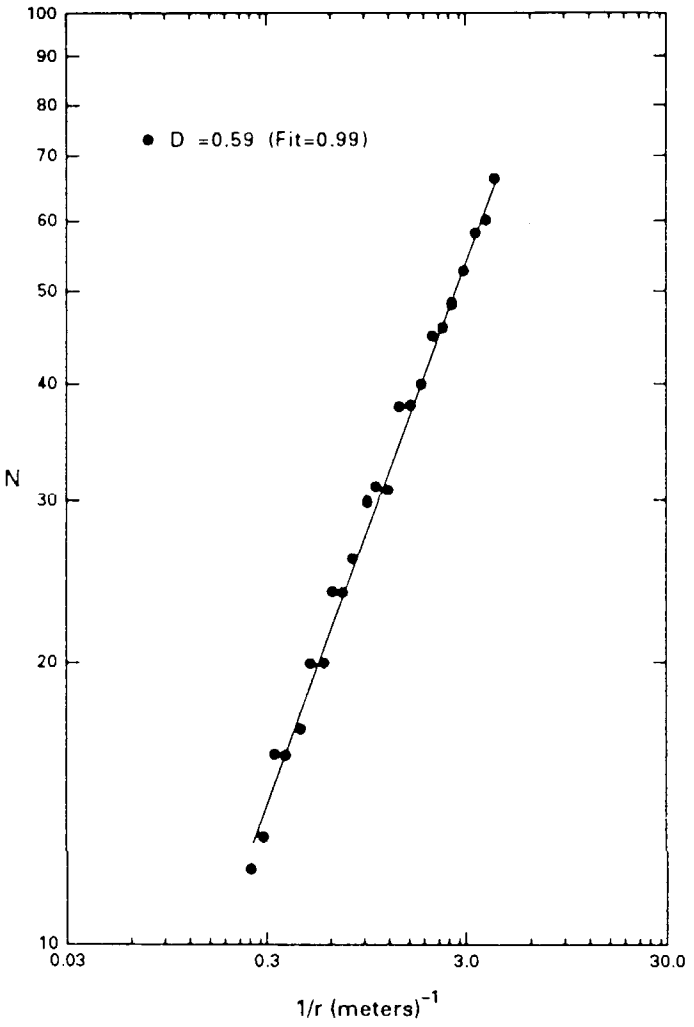

FIGURE 8.5. Fractal plot of vein spacing in Core Hole 7-18 (see Table 8.1) Perseverence mine, Juneau, Alaska; N = number of occupied cells, r = cell size, and D = fractal dimension.

TABLE 8.1. Fractal Spacing Distributions of Quartz/Gold Veins in Exploratory Cores from Perseverance Mine, Juneau, Alaska

Drill Hole Number	Fractal Dimension	Drill Hole Number	Fractal Dimension
1-26	0.52	4-14	0.48
1-27	0.45	4-202	0.51
1-28	0.52	5-5	0.45
1-29	0.41	5-38	0.58
2-2	0.43	5-39	0.51
2-23	0.58	5-40	0.62
3-3	0.55	5-41	0.42
3-20	0.54	7-7	0.47
3-21	0.49	7-18	0.59
4-4	0.51	7-19	0.55
4-12	0.46	9-31	0.47
4-13	0.48		

The significance of the fractal behavior of spacing between veins follows. If the spacing of veins is uncorrelated, then the dimension is 0.5. If the veins is evenly spaced, then the fractal dimension is 1.0. As the dimension decreases from 0.5 to 0.0, spacings become increasingly clumpy, so that at $D = 0$, data are clumped to one point. By analogy to fractional Brownian trails, this behavior is described as having a positive correlation or as being persistent (Mandelbrot, 1983). As the dimension increases from 0.5 to 1, spacings become less clumpy, more evenly spaced. Again by analogy to fractional Brownian trails, this behavior is described as having a negative correlation or as being antipersistent (Mandelbrot, 1983). The range of fractal dimension reported in Table 8.1 indicates that vein spacing can be uncorrelated, persistent, or antipersistent. The average value for all samples listed in Table 8.1 is 0.50, which indicates that on average, the vein spacing is uncorrelated. The concept of a pattern within randomness can be appreciated by constructing a fractal Cantor dust model for fracture spacing.

8.6.4. Fractal Cantor Dust Model for Fracture Spacing

A Cantor dust is a fractal set whose spacing properties are an appropriate model for the spacing properties of fractures. Generating a Cantor set is described in Mandelbrot (1983), and it is illustrated in Fig. 8.6. Begin with a solid straight line (or for illustrative purposes, a bar) and iteratively remove one or more pieces following a prescribed procedure. The procedure in Fig. 8.6a is to remove the middle one-third of the remaining pieces iteratively. This produces an ordered triadic Cantor dust whose dimension is defined by Eq. 1, where N is the number of remaining pieces, and r is the length of the pieces relative to the unit length. In this case, N equals 2 and r equals ⅓, and so D equals $\log(2)/\log(3)$ or 0.6309. The dimension of a Cantor dust is determined from the first generation, and this is the dimension for all generations. The lower size limit of the range over which the dimension is valid is the length between the two closest pieces; thus with each additional generation, the lower limit is extended. Ordered fractals are alternatively referred to as regular, symmetric, or deterministic fractals.

This Cantor dust is not a very good analog because it is too regular and its fractal dimension is slightly greater than the values we observe for spacing gold veins. Now we introduce randomness to the iterative process of forming a Cantor dust by randomly selecting which of the pieces to remove, N and r remain the same, and therefore so does the fractal dimension 0.6309. This disordered triadic Cantor dust is a much better model for the spacing of gold veins, as can be seen in Fig. 8.6b. Disordered fractals are also referred to as stochastic or random fractals. This example illustrates how and why fractals can have patterns within randomness. The fractal dimension of Cantor dusts falls between 0–1. For a given value of r, D increases from zero for $N = 1$ to 1 for $N = r$.

In strictest mathematical terms, the iterative procedure is repeated an infinite number of times to the limit as r approaches zero. Natural data sets always have some lower cutoff—a perceptibility limit—and so the number of objects is finite. Therefore for generating Cantor dusts to simulate or model spatial statistical properties of natural systems, normally only 5–10 iterations are needed. The fifth generation of the random triadic Cantor dust shown in Fig. 8.6b qualitatively evokes the pattern of fracture spacing, including variation in vein width, and quantitatively matches the spatial statistical properties of other dusts with the same fractal dimension.

The pattern of fracture spacing is controlled by unknown boundary conditions of a

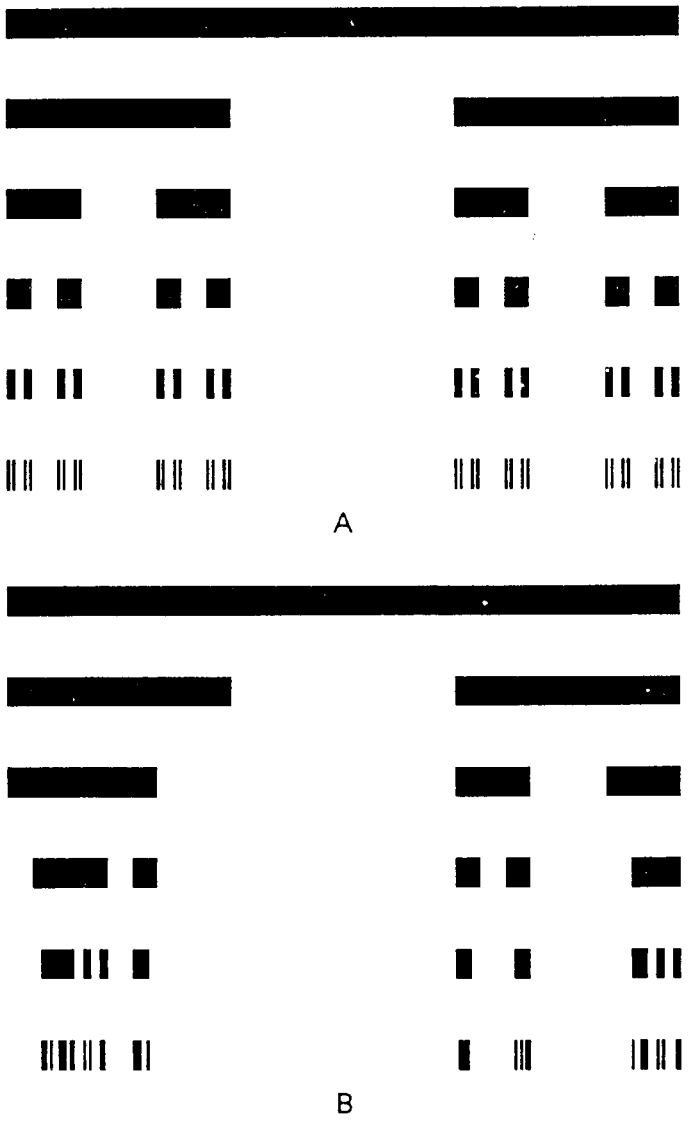

FIGURE 8.6. Triadic Cantor dust, first five generations; $D = 0.6309$. (a) Ordered; (b) disordered. (Modified from Smalley and others, 1987, Figs. 1 and 2).

complex and unknown physics that underlies the generation of fracture arrays in rock. Nevertheless it is likely that veins formed by a process akin to that of Cantor dust formation, whereby initially large blocks are broken into smaller blocks by sequential fracturing, as demonstrated for one of the two-dimensional maps that follow. The narrow range of fractal dimension (0.41–0.62) for vein spacing suggests that one physical process operated within the limits of scale sampled. Like other branches of mathematics, fractal geometry does not provide a physical or mechanistic understanding of the fracture process. Yet is provides a mathematical model and hence some insight as well as a quantitative description of the spatial properties of vein spacing. For fracture spacing, it suggests a mechanism by which larger blocks are reduced to smaller blocks by sequential fracturing, whereby survivability of large blocks (large spacings) is small. This is the mechanism revealed by dissecting fracture network maps, as described in Section 8.7.

Any number of Cantor dust models can be constructed by varying N and r to match the fractal dimension of the spacing and variation in width of veins in each drill hole. The random Cantor dust in Fig. 8.6b is a reasonable model for vein spacing in drill hole 5-40 (Table 8.1) because fractal dimensions are very close.

8.6.5. *Two-Dimensional Sampling and Analysis of Fracture Networks*

Maps of fracture traces exposed on planar surfaces are two-dimensional samples of fracture networks. Such subhorizontal exposures, ranging in area from less than 1 m^2 to more than 5000 m^2, are called pavements (Barton and Larsen, 1985; Barton and Hsieh, 1989); here the usage is extended to include subvertical and other inclined planar exposures. There are few published maps of fracture trace patterns at the scale of pavements; the only such published maps that I know of are contained in the following seven papers: Kolb and others (1970) mapped fractures in a quartz monzonite near Cedar City, Utah; Segall and Pollard (1983a, 1983b) mapped fracture traces on glacial pavements in the Givens Granodiorite in the Sierra Nevada, California; La Pointe and Hudson (1985) mapped fractures on a quarry floor in the Niagara Dolomite at Lannon, Wisconsin; Olson and Pollard (1989) mapped fractures in the Rico Limestone near Mexican Hat, Utah; Barton and Hsieh (1989) mapped fractures in the Tiva Canyon member of the Paint Brush Tuff at Yucca Mountain, Nevada; and Hill (1990) mapped fractures in the Aztec Sandstone in southern Nevada. All other published maps that I am aware of do not adequately sample the fracture network because one dimension of the map is too small [for example, mine wall maps (Chiles, 1988)] or because the range in the size of blocks bounded by fractures was considerably less than an order of magnitude. An optimal map covers an area large enough to include both ends of most of the largest traces exposed and includes at least two orders of magnitude in the length of fracture traces mapped. The maps analyzed in Chapter 8 only approach this optimal size.

Eight maps (Figs. 8.7d–g, j, m, n, and q) were prepared as a part of this study, and nine (Figs. 8.7a–c, h, i, k, l, o, and p) are taken from the literature.

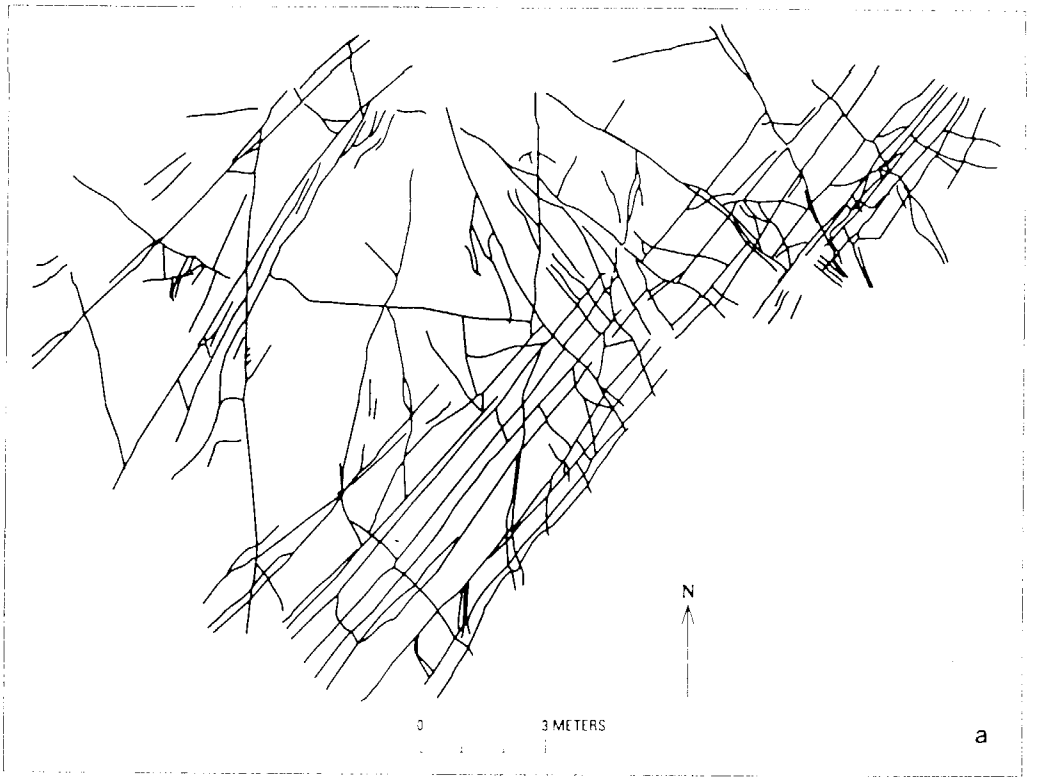

FIGURE 8.7. Fracture trace maps at various scales for 17 sites (8.7a–q). Fractal dimensions and summary descriptions of each site are given in Table 8.2.

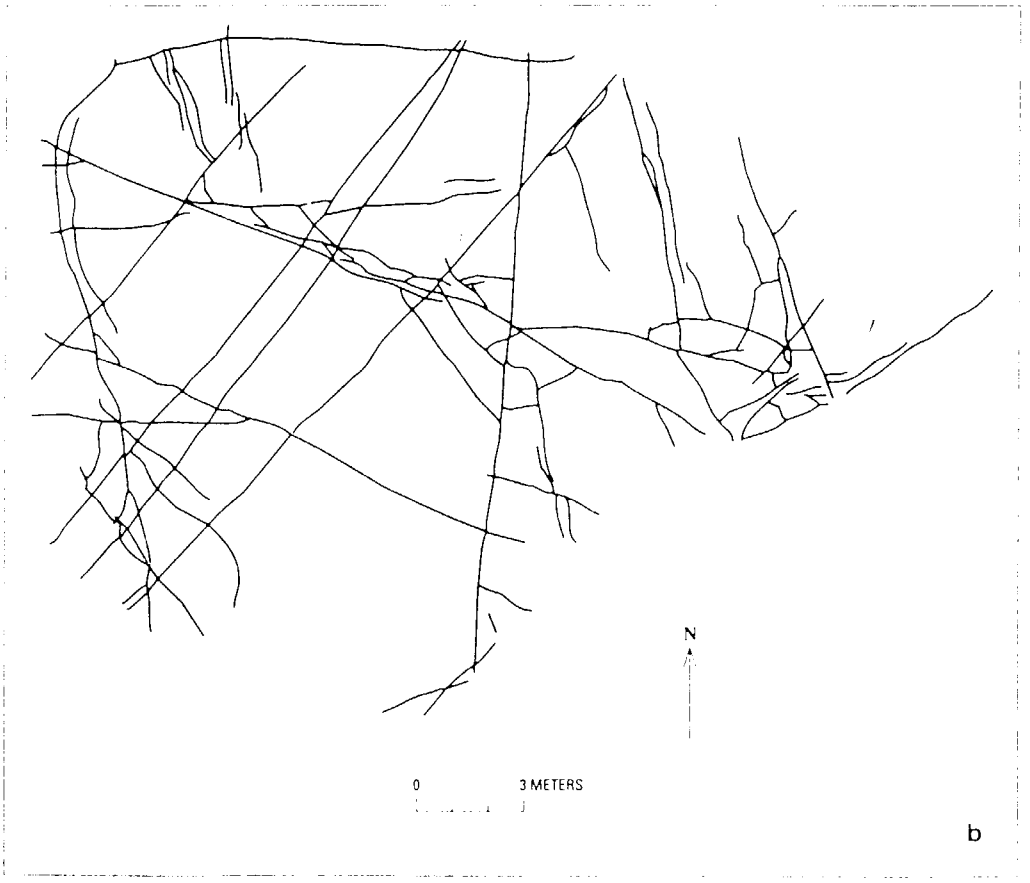

FIGURE 8.7. (*Continued*)

8.6.6. *Fracture Trace Maps*

Fracture trace maps referred to by figure number are shown in Fig. 8.7. A summary of parameters and sources for each map is given in Table 8.2. Columns in Table 8.2, from left to right, are as follows: map number, fractal dimension (box-flex method), location, rock unit designation and rock type, age of rock, scale at which fractures were mapped in the field, length of shortest fracture, length of longest fracture, and publication references. All maps are planar or subplanar, subhorizontal slices through networks of steeply dipping fractures except the map in Fig. 8.7n, which is subvertical, and maps in Figs. 8.7j and q, whose original orientations are unknown because the rocks were not in place at the time of the mapping. Several types of rock fracture are represented in this collection. Fractures on maps in Figs. 8.7a–i, l, and n formed primarily as joints, based on the absence of shear offset across them. Fractures on the map in Fig. 8.7j formed as deformation bands of reduced grain size due to shear. Fractures on the map in Fig. 8.7k formed as bands of closely packed grains across which there is no demonstrable shear; their mode of origin is unknown at this time (Hill, 1990). Fractures on maps in Figs. 8.7m, o, and p formed as faults. Faults on the map in Fig. 8.7p are transform faults. Fractures on the map in Fig. 8.7q are traces of fluid-inclusion planes as viewed in a thin section, and these exhibit no shear offset across them.

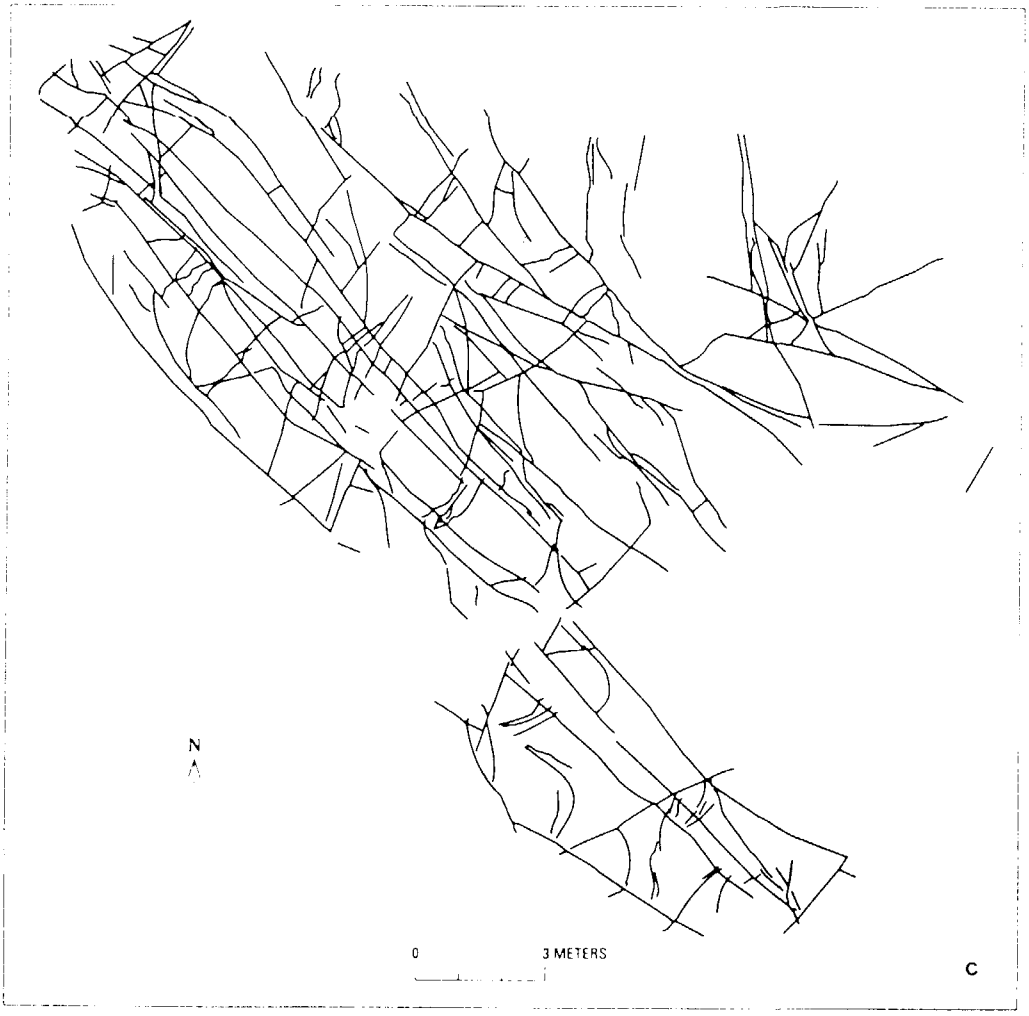

FIGURE 8.7. (*Continued*)

8.6.7. *Non Fractal Analysis Methods*

I am not aware of areal or volumetric analyses of scaling or spatial characteristics of two- or three-dimensional fracture maps. Previous studies analyzed line samples across two-dimensional maps (Hudson and Priest, 1979, 1983; and La Pointe and Hudson, 1985), a method that reduces a two-dimensional sample to a one-dimensional sample. An advantage of the fractal approach is that the data sample can be analyzed linearly, areally, or volumetrically, as appropriate to the sample.

Based on line samples of two-dimensional data sets, a number of conceptual models and synthetic fracture network generators have been proposed, all of which assume that centers of fractures are distributed in a Poisson manner; that is, there is no spatial correlation (Conrad and Jacquin, 1973; Baecher and others, 1977; Schwartz and others, 1983; Robinson, 1984; Dershowitz, 1984; La Pointe and Hudson, 1985; Long and others, 1985; Watanabe, 1986). None of these models or generators incorporates fractal scaling and spatial clustering observed on fracture network maps. Scaling is either omitted, that is, all fractures are treated as the same length, or a log-normal trace-length frequency distribution is used instead of a fractal power law trace-length frequency distribution. Barton and Hsieh (1989) present the case for fractal power law trace-length frequency distributions. The range

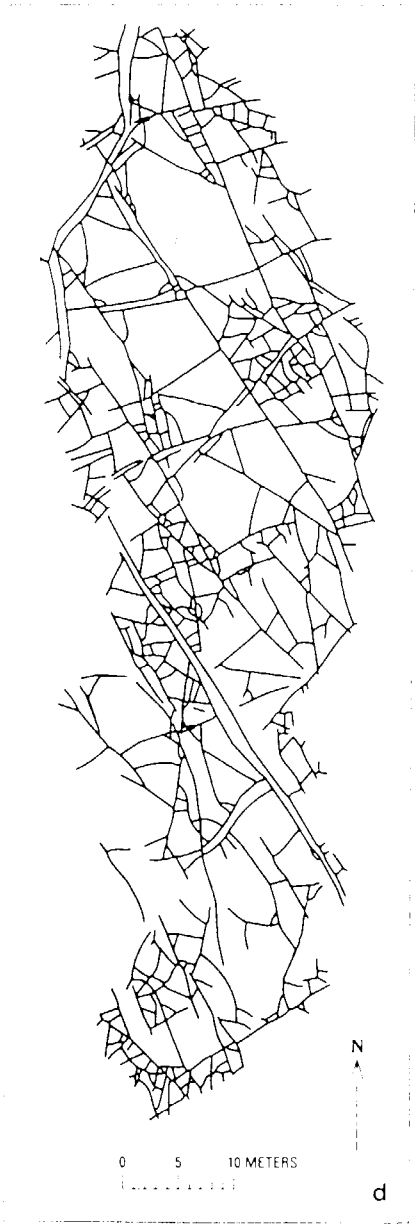

FIGURE 8.7. (*Continued*)

of scales incorporated into published models and generators is usually less than one order of magnitude, which is too limited to provide a realistic model of nature. Spatial clustering if allowed for is either Poisson or parent–daughter (Chiles, 1988), neither of which are good analogs to fractal spatial clustering. Madden (1973) studied the effect of scale and applied the renormalization group approach for modeling the spatial distribution of natural and induced microfractures in rock. This approach is closest to a fractal approach.

8.6.8. *Fractal Analysis of Scaling and Spatial-Clustering Distributions of Mapped Fracture Traces*

The fracture trace maps (Figs. 8.7a–q) were analyzed using the box-flex method, which measures both scaling and spatial clustering. The range of cell sizes used is no

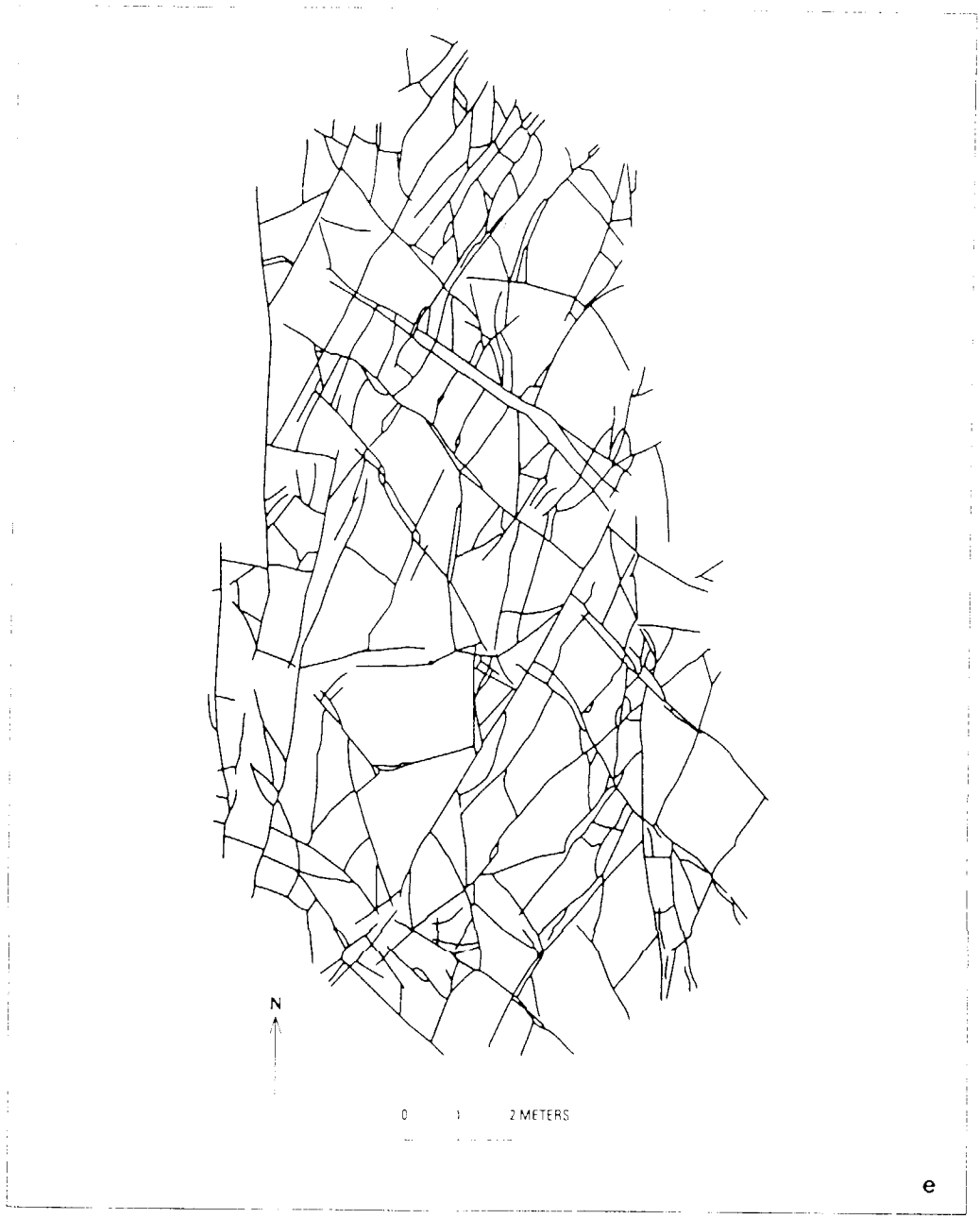

FIGURE 8.7. (*Continued*)

smaller than the shortest trace and no larger than the size at which the number of occupied cells is equal to the number of cells. Even with these limits on cell sizes, rollovers are common at both ends of the fractal plots, which I interpret to be a boundary phenomenon as we approach the upper and lower size limits of a data set. Rollovers were removed from fractal plots by the procedure of the least squares fit to the data as previously described, and the fractal dimension was calculated. Fractal plots of the number of occupied cells versus the inverse of the cell size is shown for the box-flex method in Fig. 8.8. Data points are shown for a few of the spaced best-fit lines to provide visual confirmation of the goodness of fit. Measured by a correlation coefficient, straight-line fits to the data are better than 0.99, where 1.0 is a perfect fit. The range of scales sampled on any one map is between 1–2

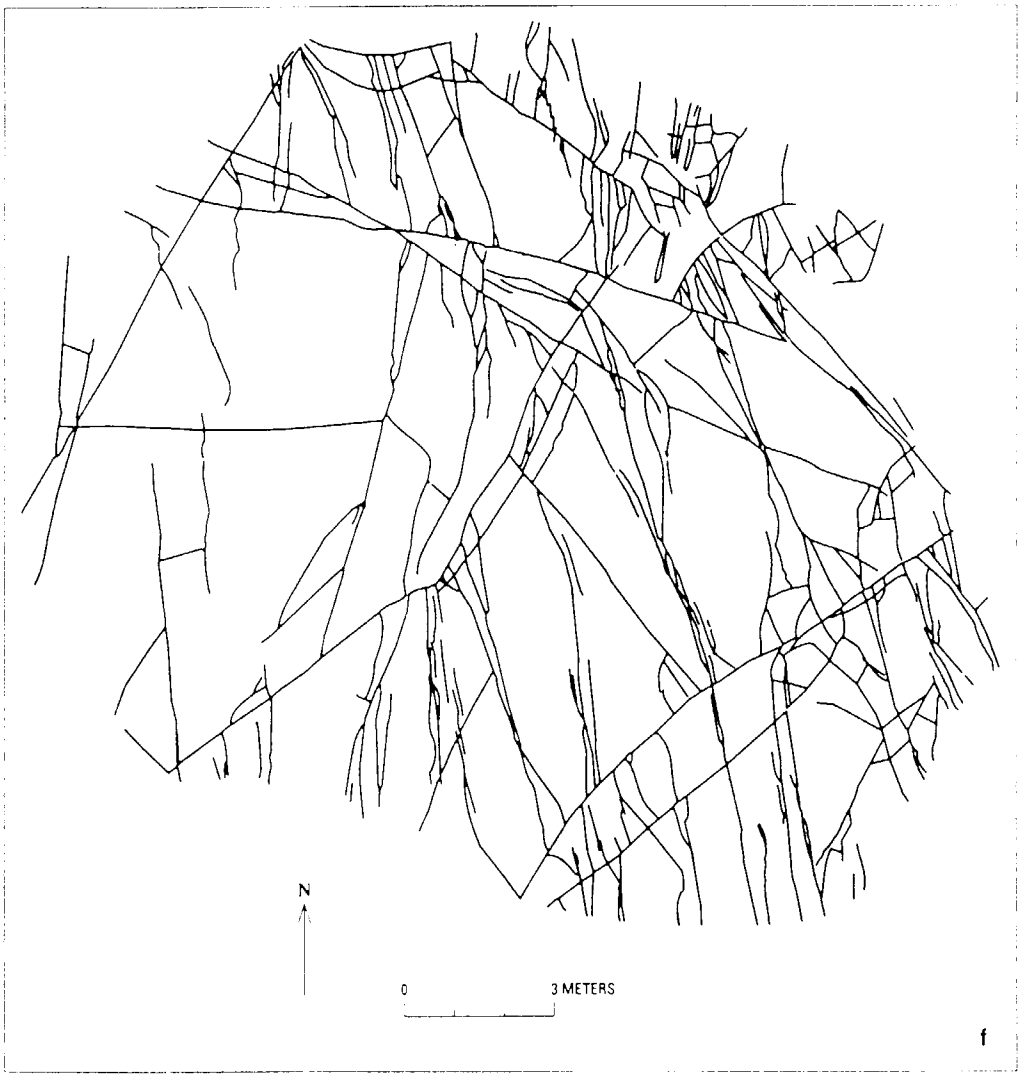

FIGURE 8.7. (*Continued*)

orders of magnitude. The total range of scales sampled in terms of cell size is approximately 0.0002–142,900 m, nearly 10 orders of magnitude.

The fractal dimension for each of the fracture trace maps is shown in Table 8.2. Results of the box-flex analysis show that the fractal dimension ranges from 1.32–1.70. Results for the Yucca Mountain maps show that there can be some change in fractal dimension within a stratigraphic unit over short lateral distances between map locations, on the order of a few tens of meters (Figs. 8.7a–c) or over longer lateral distances between map locations, on the order of a few hundred meters (Figs. 8.7d–f). There is also a difference between different stratigraphic unit—see Fig. 8.7g. The difference from one stratigraphic unit to the next arises because fractures at Yucca Mountain are stratabound at the pavement scales, with individual stratigraphic units or packets of units having different fracture patterns (Barton and Hsieh, 1989). Fractures at the scale of Fig. 8.7m are on the scale of hundreds to thousands of meters, and these cut through many stratigraphic units, including those in Figs. 8.7a–g; the fractal dimension of faults in Fig. 8.7m is 1.50, which is nearly the average (1.55) of values found for fractures in individual units at pavement scales through which they cut.

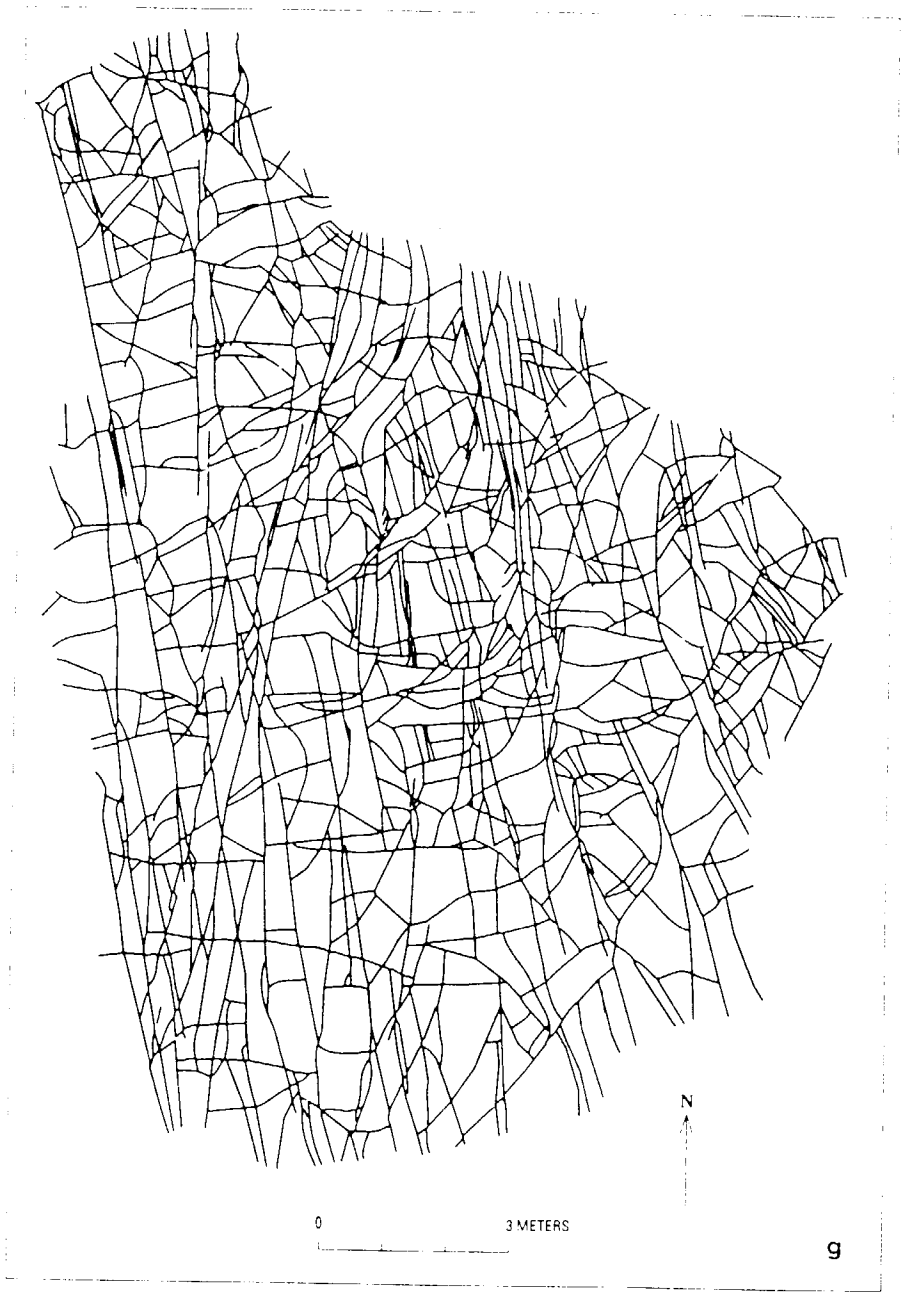

FIGURE 8.7. (*Continued*)

There are at least three fracture mechanisms in the 17 maps analyzed. Fractures on maps in Figs. 8.7a–i, l, n, and q formed primarily as joints; fractures on maps in Figs. 8.7m, o, and p formed as faults. Those on the map in Fig. 8.7j formed as deformation bands by grain size reduction in shear; and those on the map in Fig. 8.7k formed as deformation bands by more closely packing grains without grain size reduction or demonstrable shear. Table 8.2 reveals that there is apparently no correlation between mechanisms of fracture generation and the fractal dimension. This suggests that geometrical constraints on scaling and spatial clustering are independent of the mechanics that divide volumes of rock by fracturing. The narrow range in the fractal dimensions suggests an underlying physics acting over the entire range of scales investigated. The narrow range of fractal dimension

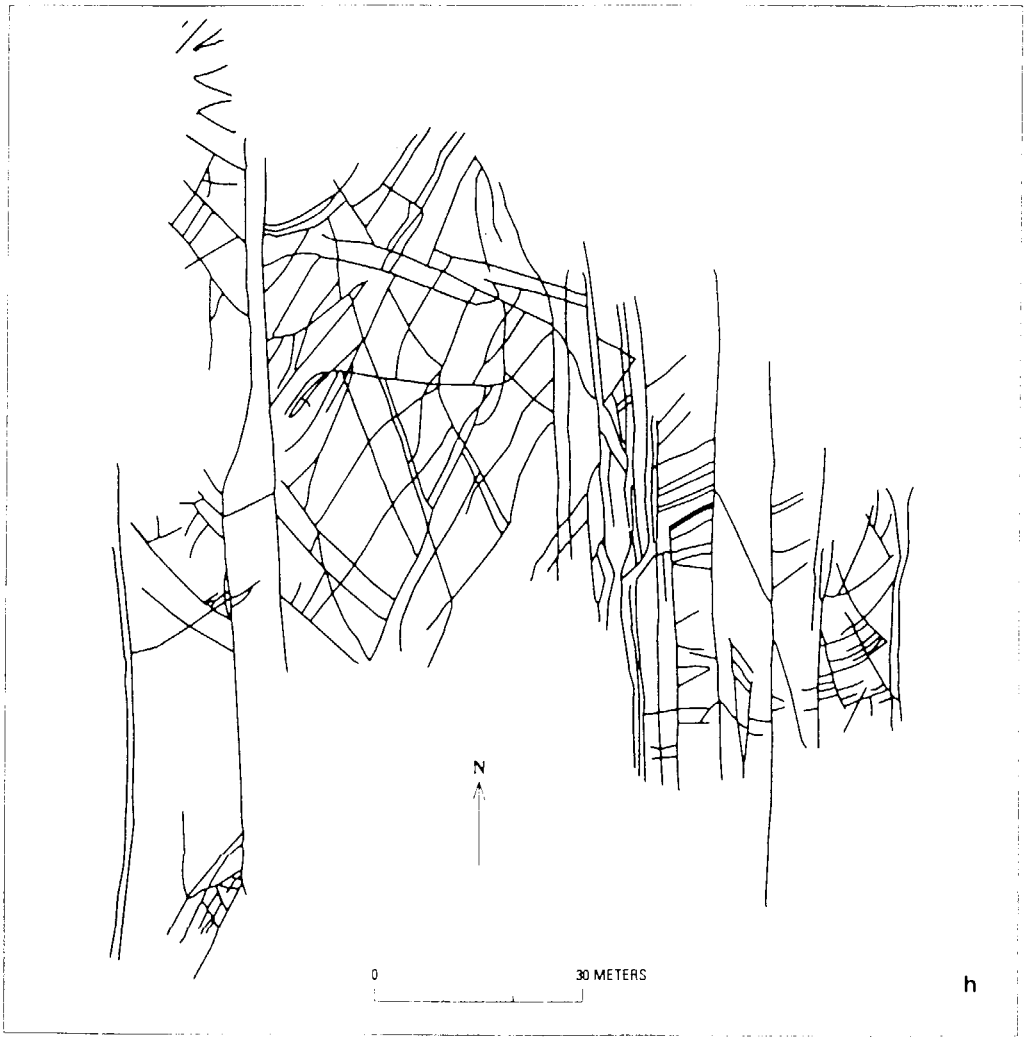

FIGURE 8.7. (*Continued*)

also suggests that geometrical scaling constraints and a common physics apply to a wide range of rock types, ages, and deformation histories represented by maps analyzed in this study.

8.7. DEVELOPMENT PATTERN OF FRACTURE NETWORKS

Fracture networks evolve from initially ordered to increasingly disordered patterns as discussed later. Fracture networks become more complex with time as new fracture generations are added to those that already exist. Fractures generations form during discrete episodes, each of which records a discrete chapter of the tectonic history. Most fracturing episodes are not accompanied by major tectonic deformations, such as folding and faulting (for example, see Barton, 1983). For fractures in a network formed as joints, the network can be disarticulated into generations of joints on the basis of abutting relations—younger fractures abut older ones. Barton and others (1986) first reported this approach for analyzing maps of joints patterns. As a typical example, the map in Fig. 8.7h was disarticulated in this way, and fractures of the same generation are given the same color (see Fig. 8.9). Note that

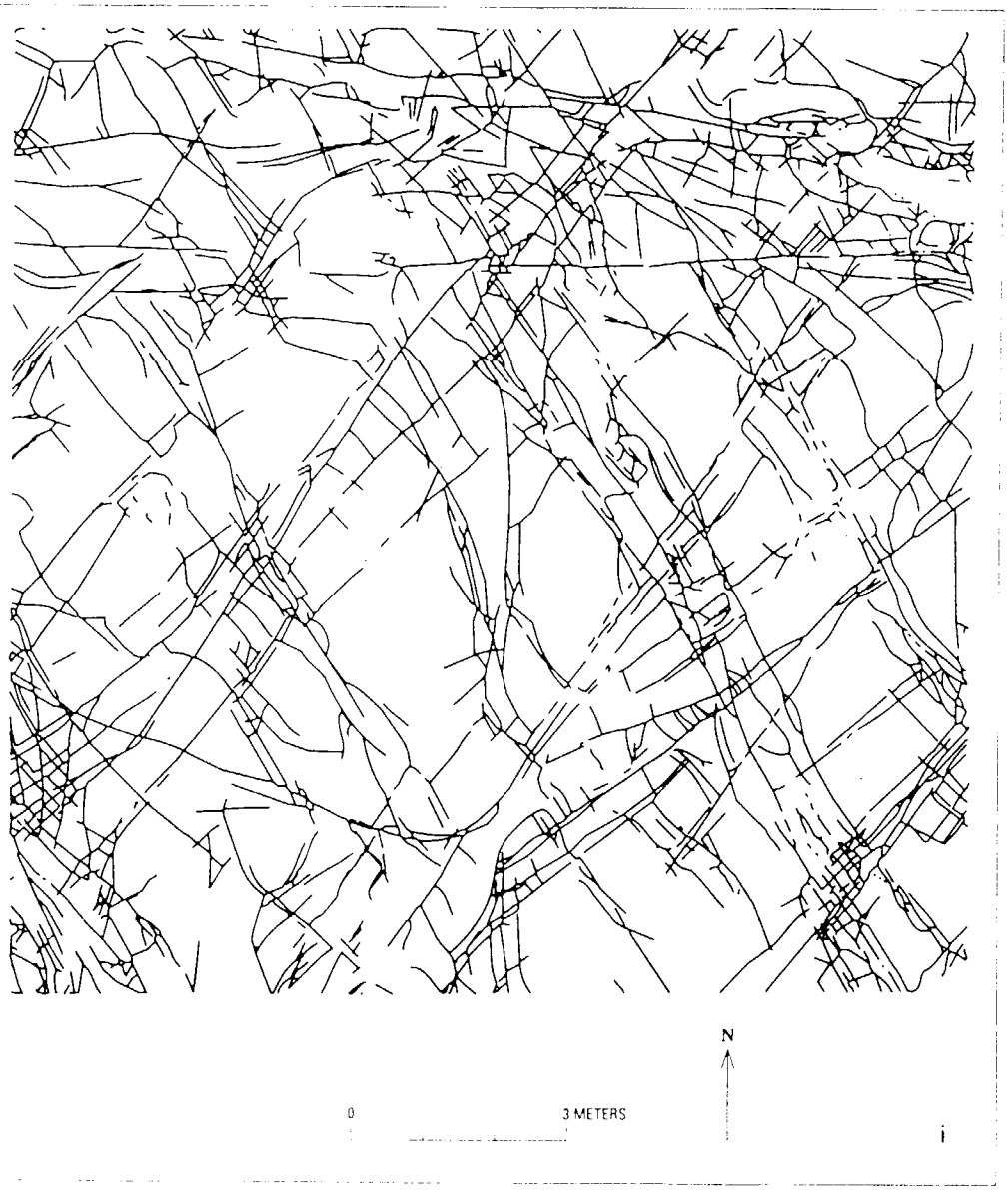

FIGURE 8.7. (*Continued*)

this approach assigns each fracture to the oldest possible generation. This interpretation of abutting relations is based on detailed observations of fracture intersections during pavement mapping. Alternative interpretations, such as the origin of multiple fractures from a shared origin or the chance passing of a younger fracture across the end of an older fracture, are not supported by my field observations.

Analysis of fracture characteristics from one generation to the next (see Figs. 8.9a–f) reveals the following general pattern of fracture network development. The first-generation fractures (see Fig. 8.9a) are long, subparallel, and network connectivity is poor. Second-generation fractures are shorter and abut first-generation fractures, generally at high angles, to form mostly large polygonal blocks (see Fig. 8.9b); network connectivity is improved. Fractures of subsequently younger generations (see Figs. 8.9b–f) are generally shorter, more diversely oriented, and increase network connectivity greatly. Younger fractures generally define small, irregular polygonal blocks bounded by older fractures. Analyzing

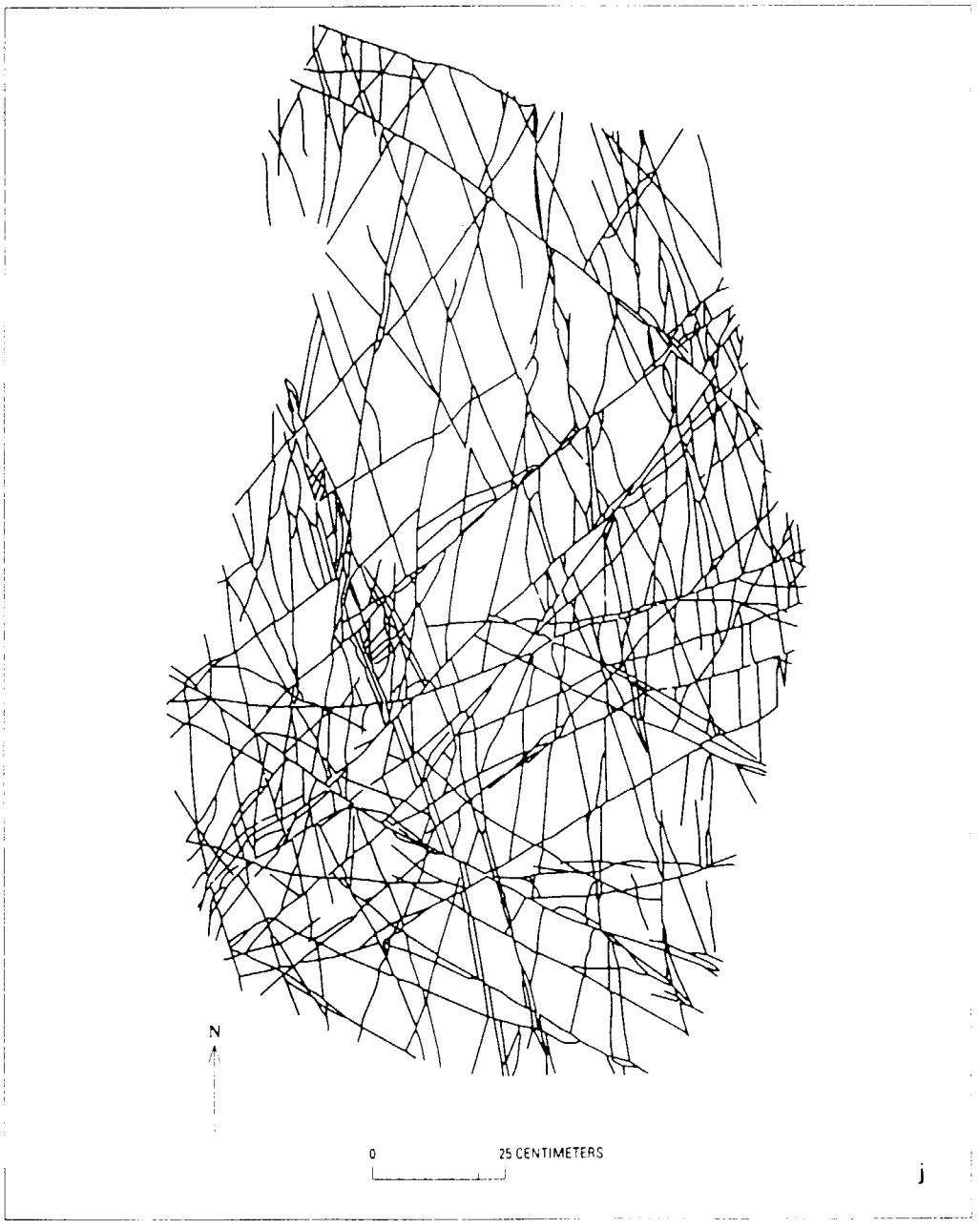

FIGURE 8.7. (*Continued*)

maps in Figs. 8.7a–d, l, and p reveals the same pattern in network evolution. Analyzing maps in Figs. 8.7e–g, i, n, and q reveals that inadequate exposure or mapping of fracture intersections or restarting the evolution by mineral infilling of previous generations renders the approach inoperable. Specifically it is inappropriate to use this approach on intersecting deformation bands (see the maps in Figs. 8.7j and k) and intersecting faults (see the maps in Figs. 8.7m and o) because younger faults truncate older fractures. Note however, that first-generation nonintersecting faults (see the map in Fig. 8.7p) are long and subparallel, as are first-generation joints shown in Fig. 8.9a.

The evolution pattern should begin anew when mineral infillings mechanically heal

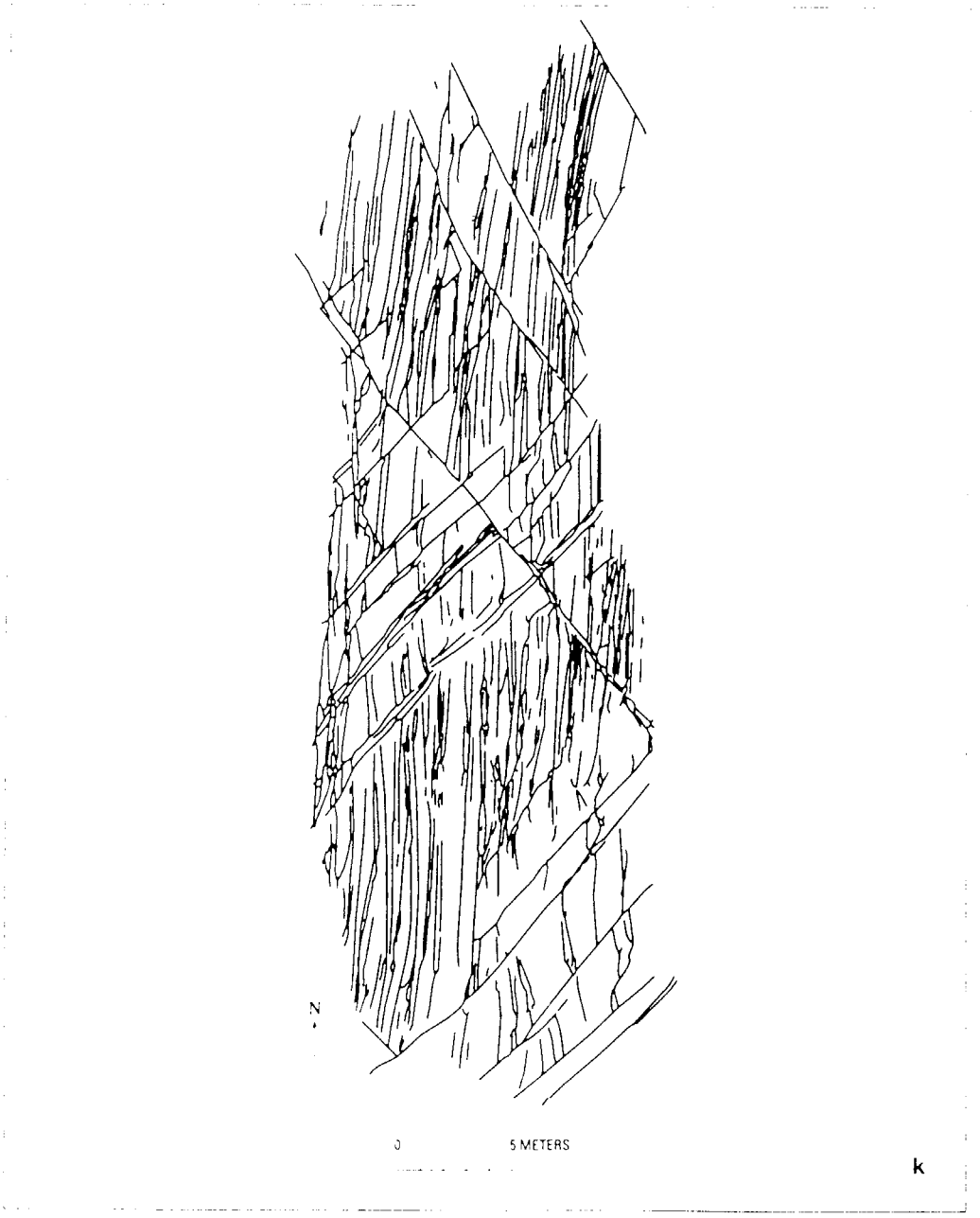

FIGURE 8.7. (*Continued*)

previous fracture generations. This predicts that one or more stages of infilling are required to permit development of highly ordered fracture patterns composed of more than one or two generations of fractures. Highly ordered fracture patterns are not observed in the stratigraphic section at Yucca Mountain, for example, where there has been little fracture healing by mineral infilling (Barton and Hsieh, 1989).

The spatial distribution of fractures within the network evolves as fractures are sequentially added to the network. The change in the box-flex fractal dimension during the evolution of the network shown in Fig. 8.9 is plotted in Fig. 8.10. The fractal dimension ranges from 1.29 for the earliest stage of network development to 1.50 for the complete

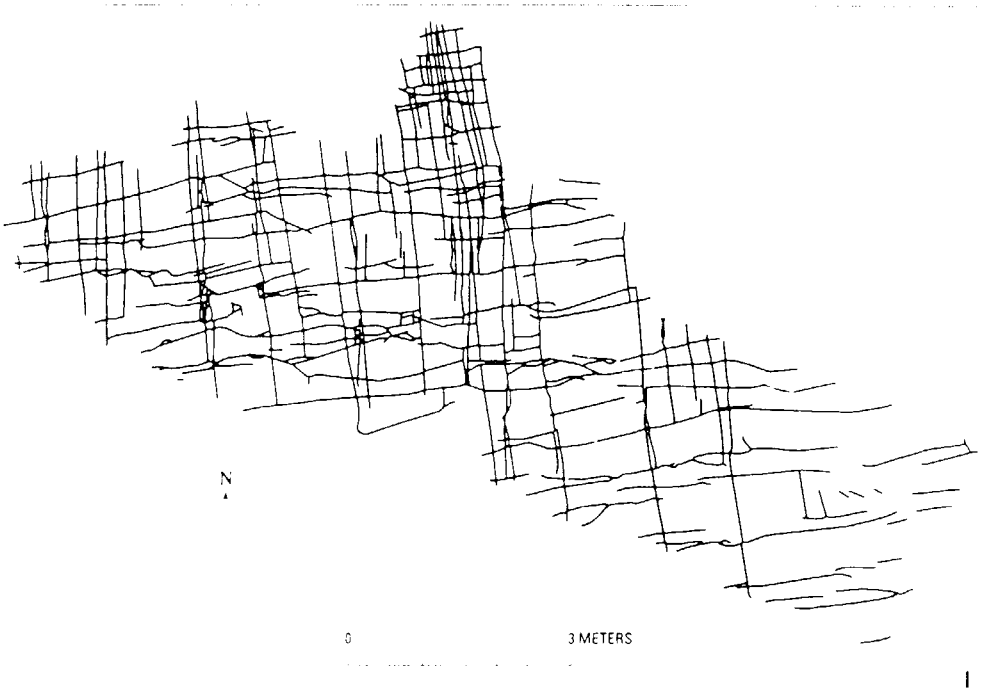

FIGURE 8.7. (*Continued*)

network. Note also that connectivity within the network is low during initial stages of development and increases as more fractures are added.

During network evolution, larger blocks are preferentially broken by subsequent fracturing (see Figs. 8.9b–f); continuing this process reduces the range of block sizes. In fault gouge, comminution by grinding also produces a fractal distribution of particle sizes with a fractal dimension of 1.6 over six orders of magnitude in scale (Sammis and Biegel, 1989), but it does not preferentially break up larger particles. The physics of grinding involves more than fracturing: In grinding the rotation and translation of particles produces large particles mechanically isolated from one another by smaller particles, and this reduces the probability of large particles being further broken up (Sammis and Biegel, 1989).

8.7.1. Percolation Threshold for Fracture Trace Maps

Fluid flow through a fracture trace network requires connectivity across the network. Connectivity for porous media has been studied using site percolation models (for a review, see Feder, 1988). An important property of percolation models is the percolation threshold below which connectivity is confined to a finite region (cluster) and above which connectivity extends across the medium (spanning cluster). For two-dimensional site percolation models, the spanning cluster always has a fractal dimension of 1.89 (Feder, 1988). By analogy to such models, I propose that the fractal dimension at the percolation threshold for fracture trace networks is approximately 1.35, based on the fractal dimension of the network consisting of the first two fracture generations shown in Fig. 8.9b. Note that the fracture trace networks in Fig. 8.7 above the percolation threshold have fractal dimensions greater than 1.35, except Fig. 8.7p, which is below the percolation threshold and has a fractal dimension of 1.32.

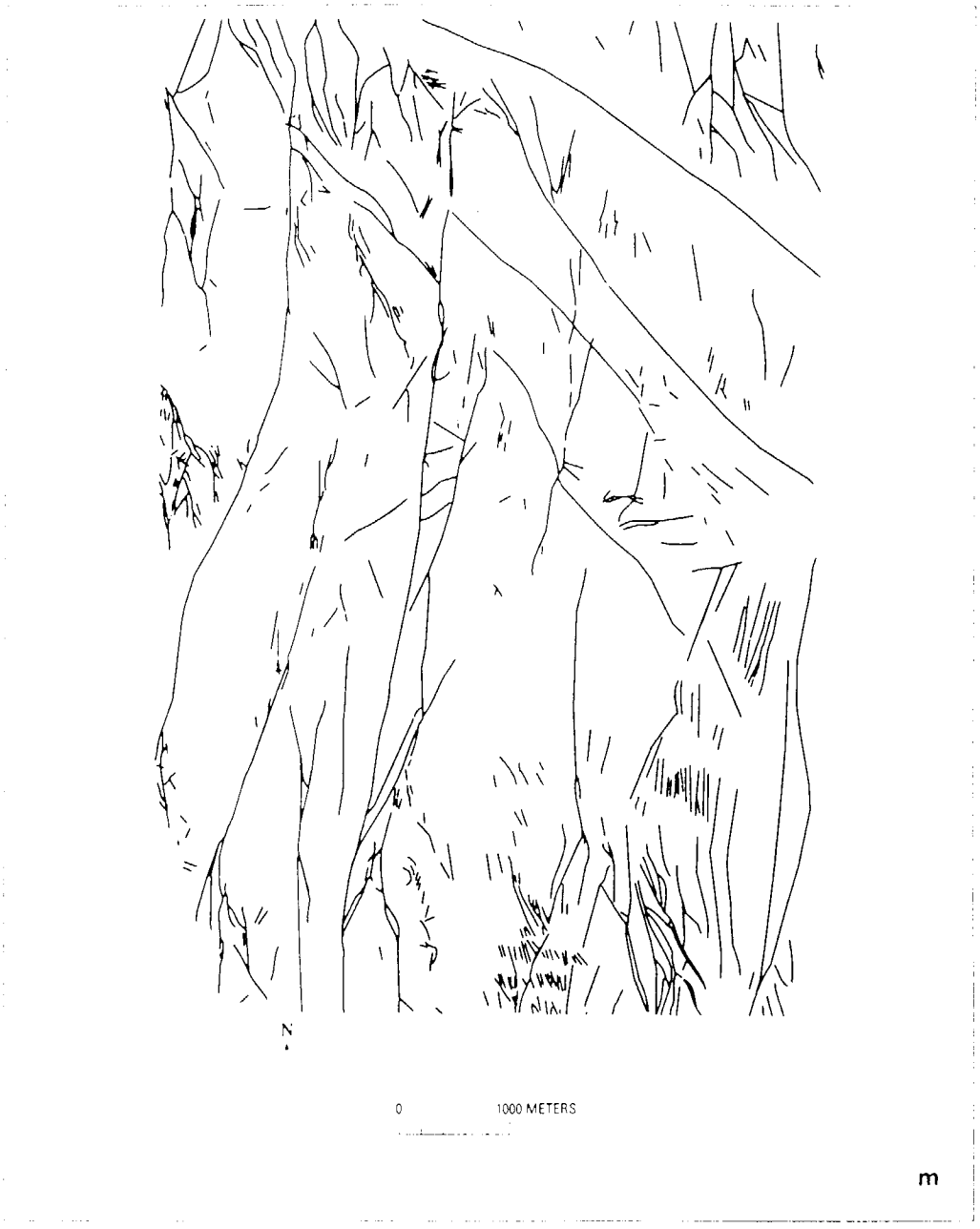

FIGURE 8.7. (*Continued*)

8.7.2. *Generating Synthetic Fracture Networks*

The evolution of fracture patterns just described is the basis for our computer generation of synthetic fracture networks (Barton and others, 1987). We have developed computer code to generate synthetic two-dimensional fracture trace networks by randomly selecting values from frequency distributions of fracture trace length, spacing, orientation, crossing, abutting, and dead-end fracture intersection distributions obtained from analyzing our fracture trace maps. The procedure is a two-dimensional analog to generating a disordered Cantor dust, in that spatial correlation is built in. This is fundamentally different from a Poisson process, which is uncorrelated and produces fracture trace patterns with a dimension of 2.

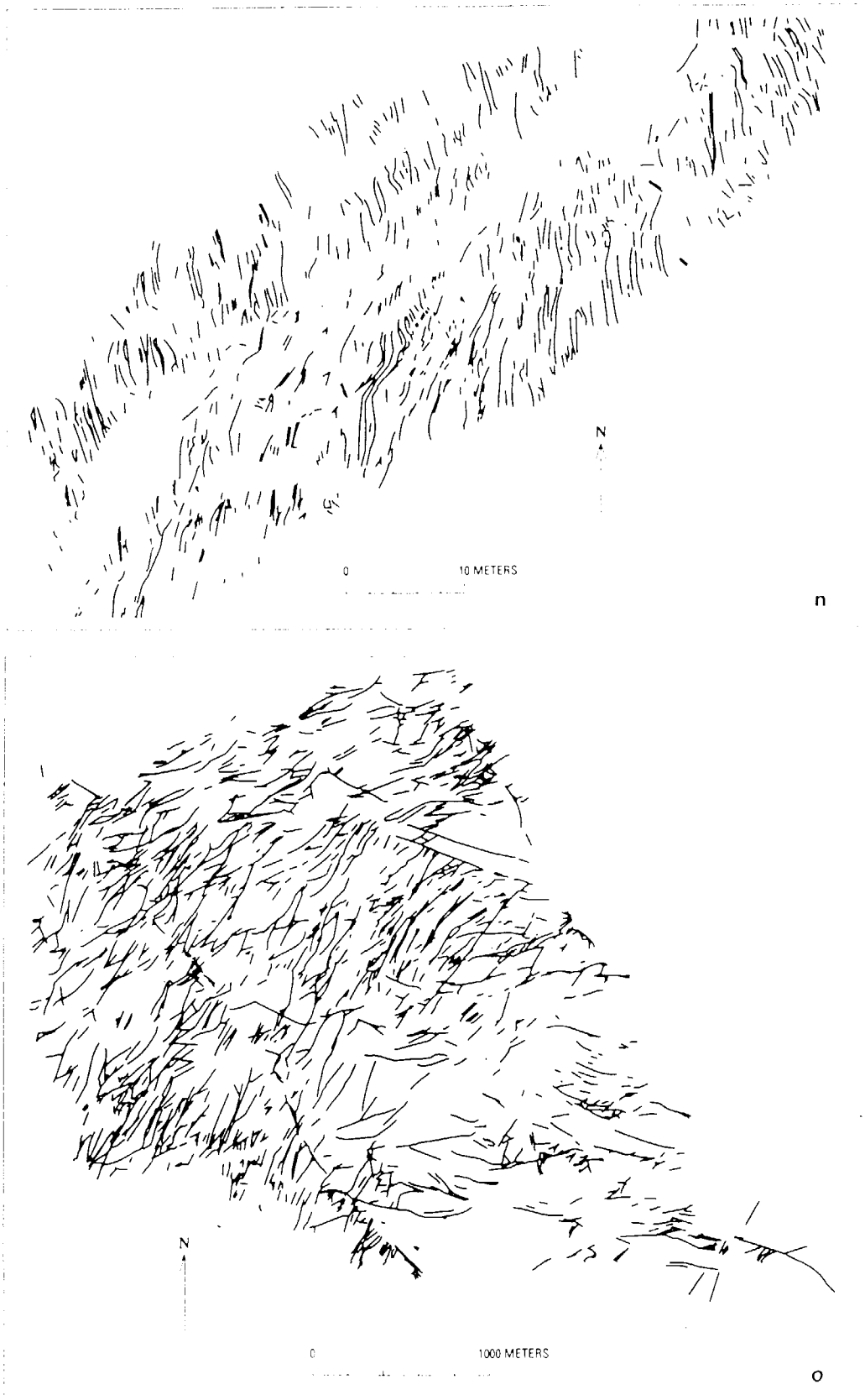

FIGURE 8.7. (*Continued*)

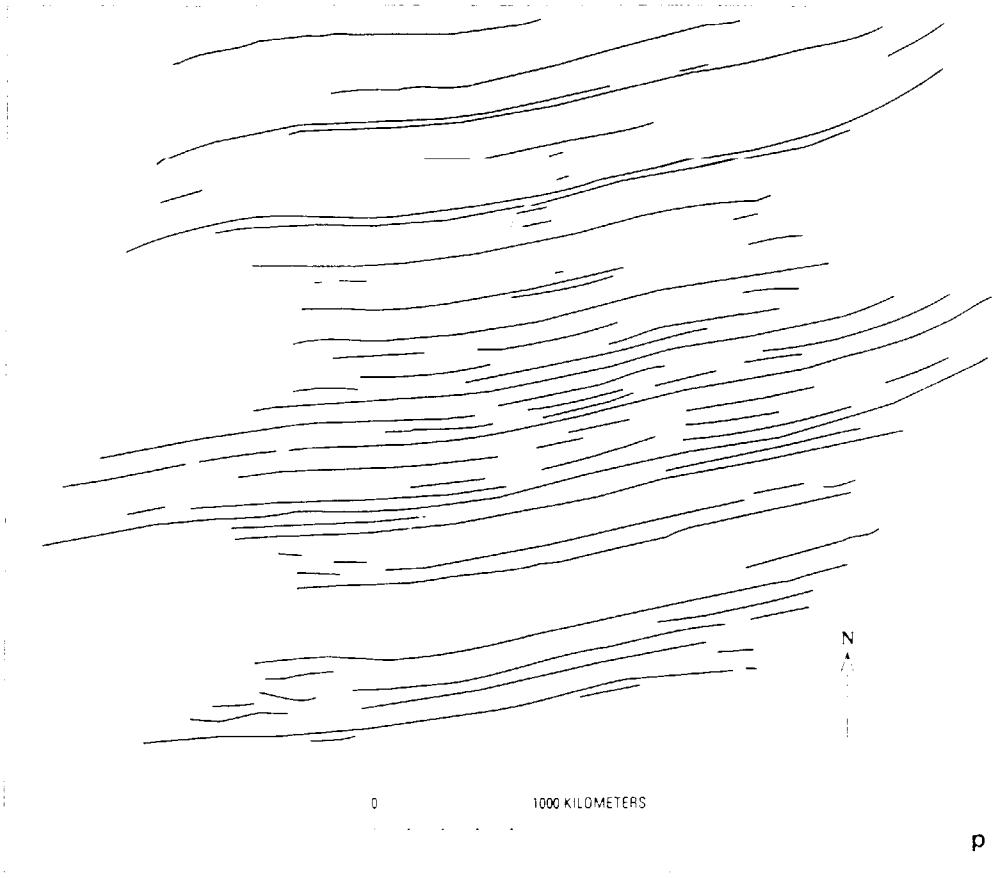

FIGURE 8.7. (*Continued*)

The basis for generating synthetic networks is the observation that fracture networks become more complex with time as younger, more diversely distributed fracture generations are added to previous generations. To define the distribution for each generation, I analyzed the sequence of fracturing in maps in Figs. 8.7a–d, and h. Relative age of the fractures is determined by abutting relations (younger abut older ones), as previously described and illustrated in Fig. 8.9. Our synthetic networks are generated by randomly selecting values of trace length, spacing, orientation, and terminations from those distributions particular to each generation. All generations after the first are initiated along traces of the preceding generation. This procedure produces synthetic networks with appropriate statistical distributions, including fractal scaling and spatial-clustering distributions. This procedure is true to the observed natural evolution of fracture networks and represents an advance beyond the Poisson process used by Dershowitz (1984), Long and others (1985), and Chiles (1988). Box-flex analysis of the synthetic network is used to verify that the fractal dimension of the synthetic network falls within the range of 1.3–1.7, which we find for fracture networks mapped in the field. Refining this approach for generating synthetic fracture networks should include further conditioning the network to observed data.

8.7.3. Extrapolating from One- and Two-Dimensional Samples

A most important characteristic of disordered, nonsymmetric, self-similar fractals is that their dimension as measured by volumetric, areal, and linear samples is each,

FIGURE 8.7. (*Continued*)

respectively, one less than the former. For example, the fractal dimension of an areal slice through a volumetric fractal of dimension 2.6 is 1.6, while that of a line sample is 0.6. Note that this relation does not hold for ordered fractals; for fractals with symmetry, such as Serpinski carpets, which are areal slices through Menger sponges (Mandelbrot, 1982), and for self-affine fractals.

As previously stated, drill holes, that is, line samples, are the most common mode of sampling scaling and spatial-clustering distributions of fractures in rock. Yet it is two- or optimally three-dimensional characterization of these properties that is needed as input to fractured rock hydrology and mechanical deformation models.

Analyses of one- and two-dimensional samples in Chapter 8 indicate that when fracture networks are shown to be fractal, it is appropriate to extrapolate from a one-dimensional sample to two dimensions. The fractal dimension of 23 linear samples of the spacing of veins at the Perseverence mine in Juneau, Alaska, ranges between 0.41–0.62, with an average of 0.50, while the dimension of an areal sample of the veins (see the map

in Fig. 8.7n) is 1.48—almost exactly an integer dimension more, as expected for disordered, nonsymmetric, self-similar fractal systems. Extrapolating the vein spacing to three dimensions predicts a volumetric fractal dimension of approximately 2.50, but this cannot be verified because there are no three-dimensional maps of the vein networks. Note that this approach averages any directional anisotropy present in the fracture network and therefore should be considered a first-order measure of the scaling properties of fracture networks.

Extrapolating to smaller sizes is also possible. Qualitative observations reveal that the number of fractures in rock continues to increase to the scale of microfractures. Fractal analysis of the smallest areas represented in this study (see the map in Fig. 8.7q) reveals that the fractal dimension ($D = 1.58$) at that size falls well within the range of 1.32–1.70 found over the range of scale of all other maps.

8.8. DISCUSSION

If fractal analyses of future fracture maps at different scales and locations have the same range as results just presented, then it is acceptable to map fractures at one scale and extrapolate spatial and statistical geometric properties to larger and smaller scales.

Once the fractal dimension of a pattern or object in nature is determined, it is possible to model that pattern or object from a single generator. A generator is the fundamental building block from which a fractal pattern or object is produced by iteratively replacing each piece of the generator with a reduced version of the generator. The task of deducing a generator for a particular fractal pattern observed in nature is not easy. One approach is to guess at the generator, as was done by King (1983) for the map pattern of traces of subsidiary faults in the immediate vicinity of large-scale fault bends. To simulate fault patterns, King (1983) proposed a nonoverlapping three-dimensional space-filling generator, but he assumed that it was never fully formed. Crosscutting fractures are common on the maps in Fig. 8.7, which suggests that a proper generator for modeling fracture trace patterns is overlapping. The generator proposed by King (1983) was for faults that did not overlap, and therefore it is not appropriate for patterns of crossing fractures. I have not succeeded in finding a generator for modeling fracture trace maps. A most promising method for deducing a fractal generator is the iterated function systems approach developed by Barnsley and Demko (1985), which systematically deduces a fractal generator for a given fractal object.

Paul Meakin (verbal communication) suggested that the behavior in Fig. 8.8 may not represent fractal behavior but rather a smooth gradual crossover between power law scaling with slopes of 1 and 2. If true, it is not appropriate to extrapolate the fractal dimension beyond length scales measured for each map in Fig. 8.7. I propose that fractures are present everywhere in rock, over many orders of magnitude in length scale, from microfractures to megascopic fractures. Thus the correct dimension for fracture networks in rock is 3 in volume space and 2 in planar (map) section. For the 17 fracture maps analyzed in Fig. 8.7, the fractal dimensions of fracture traces do not exceed 1.7. I suggest that the dimensions are less than 2 because only those fractures with apertures sufficient to render them visible were mapped. I propose that fracture networks are multifractal as a function of aperture, so that as we include fractures of successively smaller aperture, the fractal dimension of a given fracture map approaches 2. Scaling of large-aperture fracture networks will yield fractal dimensions less than 2, and such fractal dimensions correctly characterize scaling for

TABLE 8.2. Fractal Dimensions and Parameters of Fracture Trace Maps

Map Number	Fractal Dimension Box Flex Method	Location	Rock Unit/Type	Age	Map Scale	Length of Shortest Fracture (m)	Length of Longest Fracture (m)	Map Reference
8.7a	1.52	Yucca Mountain, NV	Densely welded upper lithophysal unit of the Tiva Canyon member of the Paintbrush tuff	Miocene	1:54	0.25	12	Barton and Hsieh, 1989
8.7b	1.38	Yucca Mountain, NV	Densely welded upper lithophysal unit of the Tiva Canyon member of the Paintbrush tuff	Miocene	1:104	0.50	17	Barton and Hsieh, 1989
8.7c	1.50	Yucca Mountain, NV	Densely welded upper lithophysal unit of the Tiva Canyon member of the Paintbrush tuff	Miocene	1:65	0.39	15	Barton and Hsieh, 1989
8.7d	1.61	Yucca Mountain, NV	Densely welded upper lithophysal unit of the Tiva Canyon member of the Paintbrush tuff	Miocene	1:205	0.59	42	Chap. 8
8.7e	1.59	Yucca Mountain, NV	Densely welded upper lithophysal unit of the Tiva Canyon member of the Paintbrush tuff	Miocene	1:63	0.23	8.9	Chap. 8
8.7f	1.54	Yucca Mountain, NV	Densely welded upper lithophysal unit of the Tiva Canyon member of the Paintbrush tuff	Miocene	1:74	0.24	13	Chap. 8

8.7g	1.70	Yucca Mountain, NV	Densely welded orange brick unit of the Topopah Spring member of the Paintbrush tuff	Miocene	1:55	0.20	12	Chap. 8
8.7h	1.50	Cedar City, UT	Quartz monzonite	Oligocene	1:500	1.7	110	Kolb and others, 1970
8.7i	1.60	Lannon, WI	Niagaran dolomite	Silurian	1:33	0.091	6.4	La Pointe and Hudson, 1985
8.7j	1.50	Morrison, CO	Lyons sandstone (orientation unknown)	Permian	1:3	0.12	9.7	Chap. 8
8.7k	1.58	Valley of Fire, NV	Aztec sandstone	Triassic?/ Jurassic	1:96	0.2	17	Barton and Hsieh, 1989; Hill, 1990
8.7l	1.52	Alhambra Rock, Mexican Hat, UT	Rico limestone	Penn/Permian	1:5	0.08	4.8	Olson and Pollard, 1989
8.7m	1.49	Yucca Mountain, NV	Paintbrush tuff	Miocene	1:12,000	53	6300	Scott and Bonk, 1984
8.7n	1.48	Juneau, AK	Perseverance slate (subvertical exposure)	Triassic	1:78	0.4	8	Chap. 8
8.7o	1.52	Goldhill, CO	Boulder Creek granodiorite	Precambrian	1:12,000	26	970	Goddard and Lovering, 1938
8.7p	1.32	South Atlantic seafloor	Basalt	Cretaceous–present	$1{:}4.4 \times 10^{7}$	9.9×10^{4}	6.3×10^{6}	Cande and others, 1988
8.7q	1.58	Timmins, Ontario	Albite, quartz, scheelite	Archean	1:65	5×10^{-4}	1.3×10^{-2}	Chap. 8

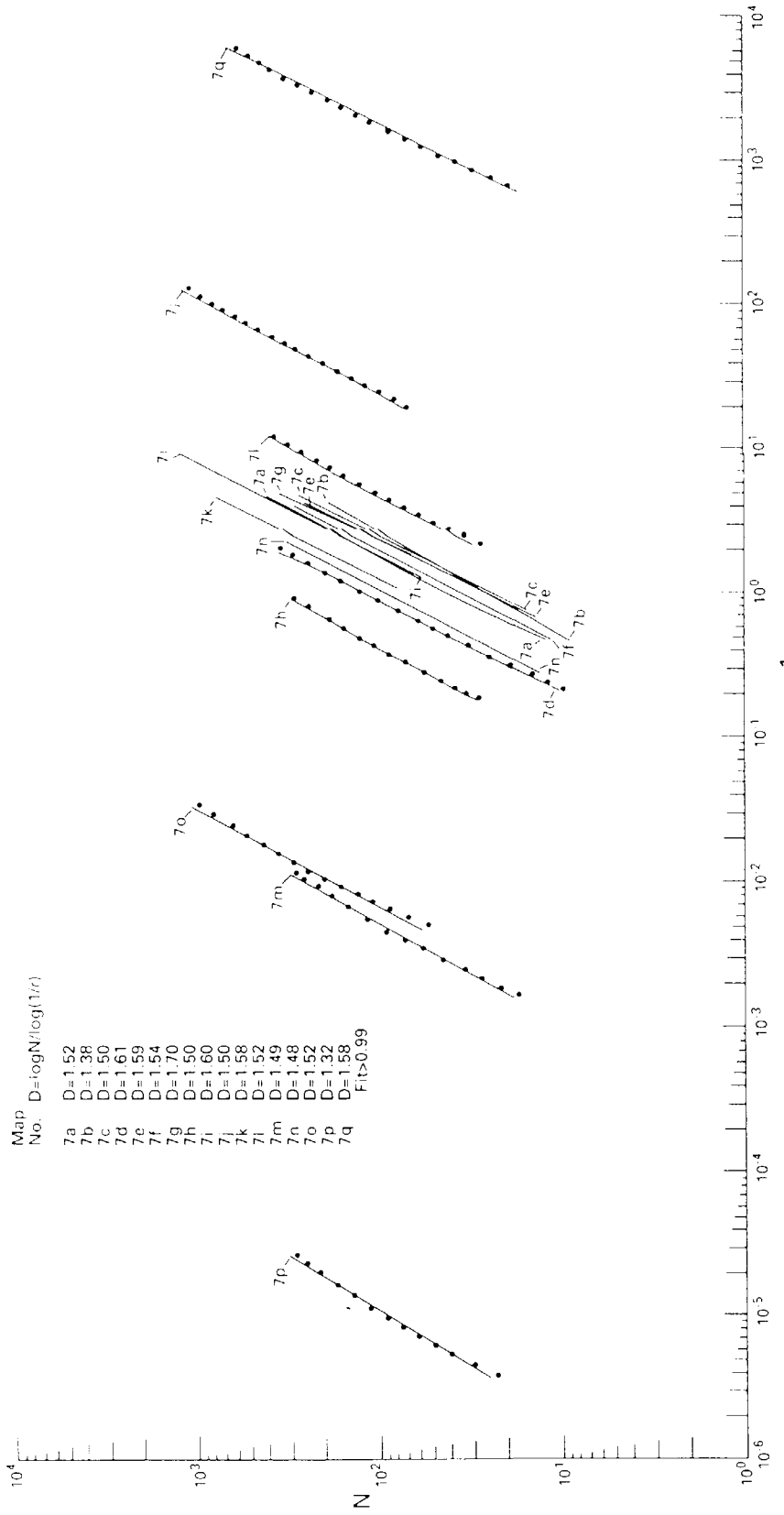

FIGURE 8.8. Fractal plot for fracture trace maps (Figs. 8.7a–q) using the box-flex method. N = number of occupied cells, r = cell size, and D = fractal dimension. The continuous stream of data points generated for each analysis by the box-flex method are not shown; every third data point is shown for analyses that do not overlap on plot.

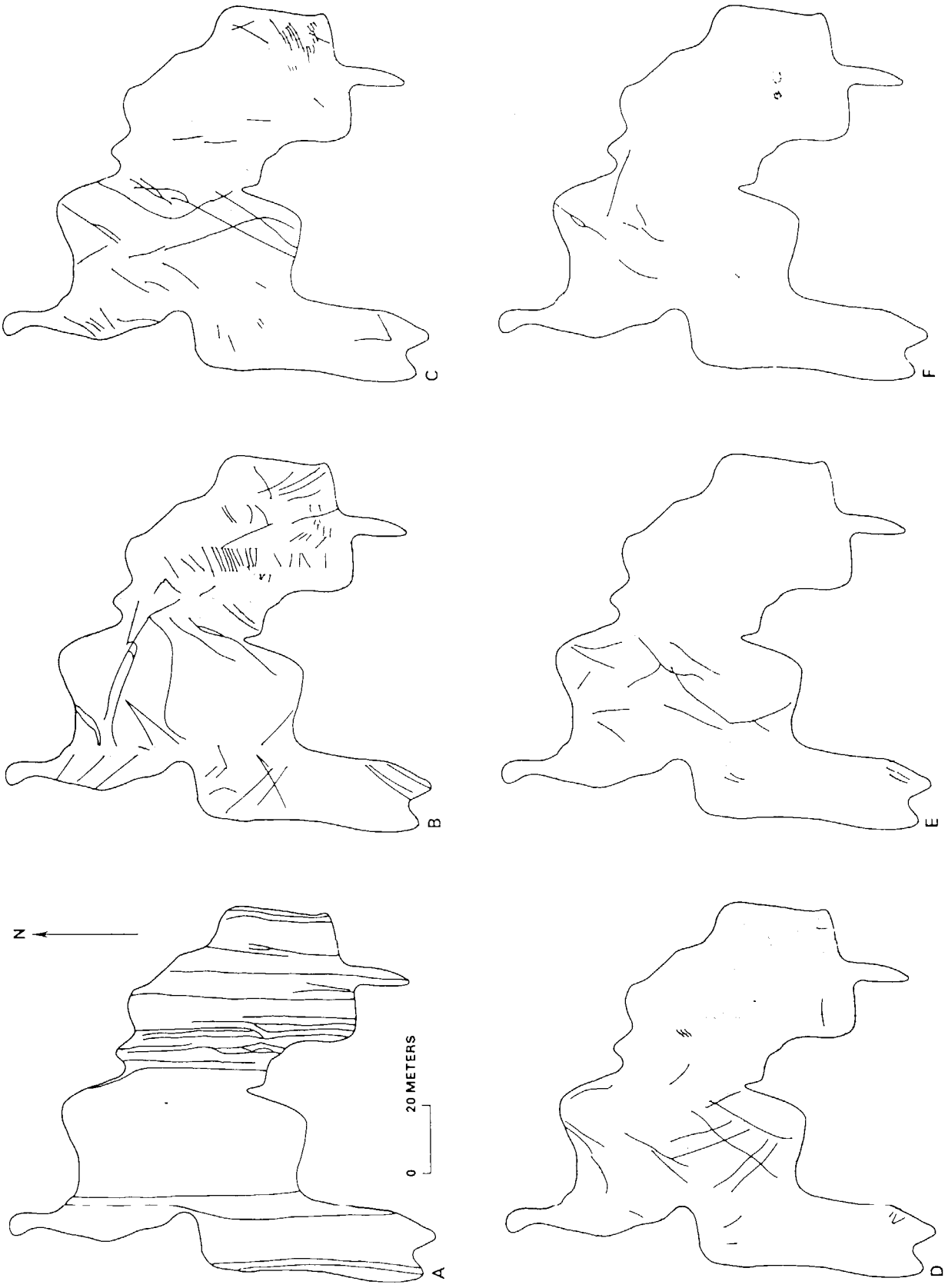

FIGURE 8.9. Fracture trace map in Fig. 8.7h dissected to show fractures grouped into six relative age generations based on abutting relations. (a) First generation fractures; (b–f) fractures added by generation; latest generation shown in black, previous generations shown in gray.

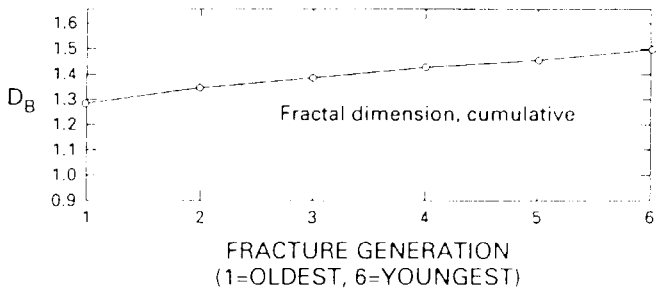

FIGURE 8.10. Plot of the box-flex fractal dimension versus fracture generation for the evolution of the fracture trace map in Fig. 8.7h shown in Fig. 8.9. Curve shows fractal dimension of cumulative pattern as each succeeding generation is added.

studies of fluid flow through fracture networks. However calculations of storativity in fracture networks should assume a dimension of 3 in volume space and 2 in planar section.

8.9. CONCLUSIONS

Fractal dimensions for scaling and spatial-clustering of fractures along drill holes prove to be random Cantor dusts with fractal dimensions ranging from 0.42–0.62 over a range of four orders of magnitude. The fractal dimensions for scaling and spatial clustering of fracture trace maps range from 1.38–1.70 over nearly ten orders of magnitude in length scale. A fracture network sampled by both drill holes and mapping a planar outcrop revealed fractal dimensions of 0.50 and 1.48, respectively, nearly an integer dimension difference, as is expected for disordered, nonsymmetric, statistically self-similar fractal patterns. This result suggests that extrapolating from one-dimensional samples to planar or volumetric dimensional samples is not unreasonable for fracture networks. The change of fractal dimension from the iterative addition of new fractures during the evolution of fracture networks is investigated by disarticulating and then reconstructing the evolution of a fracture trace map. Analysis reveals that the fractal dimension of the network increases with the addition of each successive generation of fractures. Thus the fracture network exhibits multifractal behavior with time. The evolution of fracture networks is proposed as a physical model for constructing synthetic fracture networks. A fractal dimension of 1.35 is found for an evolving fracture trace network at or just beyond the percolation threshold. There is no three-dimensional (volumetric) analysis because of a lack of data.

ACKNOWLEDGMENTS

I am indebted to the following individuals for their help in fracture mapping: Eric Larsen, Thomas A. Howard, and Patricia E. Baechle of Fenix & Scisson, Inc., maps in Figs. 8.7a, c, d, b, and f respectively; William R. Page and Constance K. Throckmorton of the US Geological Survey, maps in Figs. 8.7g and e, respectively; Marc B. Gamble, of Colorado College, the map in Fig. 8.7j; Robin E. Hill, of the University on Nevada, Las Vegas, the map in Fig. 8.7k; and Dominic Channer of the university of Toronto, the map in Fig. 7.8q. I am most indebted to Thomas A. Schutter of the US Geological Survey, who programmed the box algorithms used to produce the fractal plots and calculate the fractal dimensions presented in Chapter 8. William D. Stansbury of the Colorado School of Mines aided in the fractal analyses summarized in Table 8.1. Petro A. Zlatev of the Colorado School of Mines, Paul R. Herring, and William J. Thomas of the University of Colorado,

Boulder aided in the fractal analyses summarized in Table 8.2. Glen Miller of WGM-Echo Bay Mining Company generously provided data for the fractal analysis of vein spacing in the Perseverence mine. The photograph in Fig. 8.1d was taken by Kenneth Bradbury of the Wisconsin Geological and Natural History Survey.

REFERENCES

Baecher, G. B., Lanney, N. A., and Einstein, H. H., *Statistical Description of Rock Properties and Sampling*, Proceedings of the 18th US Symposium on Rock Mechanics, Colorado School of Mines Press, Golden, CO, American Institute of Mining Engineers, 1977, pp. 5c1–5c8.

Barnsley, M. F., and Demko, S., *Iterated Function Systems and the Global Construction of Fractals*, *Proc. Roy. Soc. London Series A* **399**, 243 (1985).

Barton, C. A., and Zoback, M. D., Self-similar distribution and properties of macroscopic fractures at depth in crystalline rocks in the Cajon Pass scientific drill hole, *J. Geophys. Res.* **97**, **B4**, 5181 (1992).

Barton, C. C., "Systematic Jointing in the Cardium Sandstone along the Bow River, Alberta, Canada," Ph.D. diss., Yale University, 1983.

———, Fractal characteristics of fracture networks in rock, in *Rock Mechanics—Contributions and Challenges*, 31st US Symposium on Rock Mechanics (A. A. Balkema, Rotterdam, 1990).

Barton, C. C., and Larsen, E., Fractal geometry of two-dimensional fracture networks at Yucca Mountain, southwest Nevada, in *Fundamentals of Rock Joints*, Proceedings of the International Symposium on Fundamentals of Rock Joints, Bjorkliden, Lapland, Sweden (O. Stephannson, ed.) (Centek Publishers, Lulea, Sweden, 1985), pp. 74–84.

Barton, C. C., Gott, C. B., and Montgomery, J. R., Fractal scaling of fracture and fault maps at Yucca Mountain, southern Nevada (abs.), *Eos Trans. Am. Geophys. Union* **67**, **44**, 870 (1986).

Barton, C. C., and Hsieh, P. A., *Physical and Hydrologic Flow Properties of Fractures*, Field Trip Guidebook T385, 28th International Geological Congress (American Geophysical Union, Washington, DC, 1989).

Barton, C. C., Page, W. R., and Larsen, E., Pattern of development of fracture networks, *Geol. Soc. Am. Abstr. Programs* **18**, **6**, 536 (1986).

Barton, C. C., Schutter, T. A., Page, W. R., and Samuel, J. K., Computer generation of fracture networks for hydrologic-flow modeling, *Eos Trans. Am. Geophys. Union* **68**, **44**, 1295 (1987).

Barton, C. C., and Scholz, C. H., Consequences of fractal distributions of fracture length and aperture on fluid flow through fractured rock, in press.

Bear, J., *Dynamics of Fluids in a Porous Media* (American Elsevier, New York, 1972).

Brown, S. R., Measuring the dimensions of self-affine fractals: The example of rough surfaces, in this volume, Chap. 4.

Chiles, J. P., Fractal and geostatistical methods for modeling of a fracture network, *Math. Geol.* **20**, 631 (1988).

Conrad, F., and Jacquin, C., Representation d'un reseau bi-dimensionnel de fractures par un modele probabiliste. Application au calcul des grandeurs geometriques des blocks matriciels, *Rev. Institut Fr. Pet.* **28**, 843 (1973).

DeMarsily, G., *Flow and Transport in Fractured Rocks: Connectivity and Scale Effect*, International Association of Hydrologists, Memoirs, Vol. 17, Part 2 (International Association of Hydrogeologists, 1985), pp. 267–77.

Dershowitz, W. S., "Rock Joint Systems," Ph.D. diss., Massachusetts Institute of Technology, 1984.

Feder, J., *Fractals* (Plenum Press, New York, 1988).

Goddard, E. N., and Lovering, T. S., "Geologic Map of the Gold Hill Mining District, Boulder County, Colorado" (US Geological Survey, 1938).

Hausdorff, F., Dimension und ausseres Mass, *Math. Ann.* **79**, 157 (1919).

Hill, R. E., "Analysis of Deformation Bands in the Aztec Sandstone," Valley of Fire State Park, Nevada, M.S. thesis, University of Nevada, Las Vegas, 1990.

Hirata, T., Fractal dimension of fault systems in Japan: Fractal structure in rock fracture geometry at various scales, *Pure Appl. Geophys.* **131**, 290 (1989).

Hohn, M. E., *Geostatistics and Petroleum Geology* (Van Nostrand Reinhold, New York, 1988).

Hudson, J. A., and Priest, S. D., Discontinuities and rock mass geometry, *Int. J. Rock Mech. Min. Sci. Geomech. Abstr.* **16**, 339 (1979).

———, Discontinuity frequency in rock masses, *Int. J. Rock Mech. Min. Sci. Geomech. Abstr.* **17**, 279 (1983).

Journel, A. G., and Huijbregts, C. J., *Mining Geostatistics* (Academic Press, London, 1978).

King, G. C. P., The accommodation of large strains in the upper lithosphere of the earth and other solids by self-

similar fault systems: the geometric origin of b-value, *Pure Appl. Geophys.* **121**, 761 (1983).

Kolb, C. R., Farrell, W. J., Hunt, R. W., and Curro, J. R., Jr., "Geological Investigation of the Mine Shaft Sites, Cedar City, Utah," US Army Engineer Waterways Experiment Station, Report MS-2170, 1970.

Korvin, G., Fractured but not fractal: Fragmentation of the Gulf of Suez basement, *Pure Appl. Geophys.* **131**, 290 (1989).

Kulander, B. K., Barton, C. C., and Dean, S. L., "Applications of Fractography to Core and Outcrop Investigations," US Department of Energy METC SP-79/3, 1979.

La Pointe, P. R., Analysis of the spatial variation in rock mass properties through geostatistics, in *Rock Mechanics—a State of the Art*, Proceedings, 21st US Symposium on Rock Mechanics (D. A. Summers, ed.) (University of Missouri Press, Rolla, 1980), pp. 570–80.

La Pointe, P. R., A method to characterize fracture density and connectivity through fractal geometry, *Int. J. Rock Mech. Min. Sci. Geomech. Abstr.* **25**, 421 (1988).

La Pointe, P. R., and Hudson, J. A., "Characterization and Interpretation of Rock Mass Joint Patterns," Geological Society of America, Special Paper 199, 1985.

Long, J. C. S., Endo, H. K., Karasaki, K., Pyrack, L., MacLean, P., and Witherspoon, P. A., Hydrologic behavior of fracture networks, in *Hydrology of Rocks of Low Permeability*, International Association of Hydrologists, Memoirs, Vol. 17, Part 2 (International Association of Hydrogeologists, 1985), pp. 449–62.

Madden, T. R., Microcrack connectivity in rocks: A renormalization group approach to the critical phenomena of conduction and failure in crystalline rocks, *J. Geophys. Res.* **88**, 585 (1973).

Majer, E. L., McEvilly, T. V., Eastwood, F. S., and Myer, L. R., Fracture detection using P- and S-wave VSP's at the Geysers geothermal field, *Geophysics* **53**, 76 (1988).

Mandelbrot, B. B., *The Fractal Geometry of Nature* (W. H. Freeman, New York, 1982).

Manning, C. E., Fractal clustering of metamorphic veins, *Geology* **22**, 335 (1994).

Olson, J., and Pollard, D. D., Inferring paleostress from natural fracture patterns: A new method, *Geology* **17**, 345 (1989).

Oxaal, U., Murat, M., Boger, F., Aharony, A., Feder, J., and Jossag, T., Viscous fingering on percolation structures, *Nature* **329**, No. 6134, 32 (1987).

Paillet, F. L., Use of geophysical well-logs in evaluating crystalline rocks for siting of radioactive waste repositories, *Log Anal.* **32**, 85 (1991).

Priest, S. D., and Hudson, J. A., Estimation of discontinuity spacing and trace length using scanline surveys, *Int. J. Rock Mech. Min. Sci. Geomech. Abstr.* **13**, 135 (1976).

———, Estimation of discontinuity spacing and trace length using scanline surveys, *Int. J. Rock Mech. Min. Sci. Geomech. Abstr.* **18**, 183 (1981).

Pruess, S. A., Some remarks on the numerical estimation of fractal dimension, in this volume, Chap. 3.

Ramirez, A. L., and Daily, W. C., Evaluation of alternate geophysical tomography in welded tuff, *J. Geophys. Res.* **92**, **8**, 7843 (1987).

Robinson, P. C., "Connectivity, Flow, and Transport in Network Models of Fractured Media," Ph.D. diss., Oxford University, 1984.

Sammis, C. G., and Biegel, R. L., Fractals, fault-gouge, and friction, *Pure Appl. Geophys.* **131**, 255 (1989).

Schwartz, F. W., Smith, L., and Crow, A. S., A stochastic analysis of macroscopic dispersion in a fractured media, *Water Resour. Res.* **19**, 1253 (1983).

Scott, R. B., and Bonk, J., "Preliminary Geologic Map of Yucca Mountain, Nye County, Nevada, with Geologic Sections," US Geological Survey Open-File Report 84-491, 1984.

Segall, P., and Pollard, D. D., Joint formation in granitic rock of the Sierra Nevada, *Geol. Soc. Am. Bull.* **94**, 563 (1983a).

———, Nucleation and growth of strike slip faults in granite, *J. Geophys. Res.* **88**, **B1**, 555 (1983b).

Smalley, R. F., Jr., Chatelain, J.-L., Turcotte, D. L., and Prévot, R., A fractal approach to the clustering of earthquakes: Applications to seismicity of the New Hebrides, *Bull. Seism. Soc. Am.* **77**, 1368 (1987).

Thorp, R. K., Watkins, B. J., and Ralph, W. E., Strength and permeability of an ultra-large specimen of granitic rock, in *Rock Mechanics Theory—Experiment—Practice*, Proceedings of the 24th US Rock Mechanics Symposium (C. C. Mathewson, ed.) (Texas A&M University Press, College Station, 1983), pp. 511–18.

Velde, B., Dubois, J., Touchard, G., and Badri, A., Fractal analysis of fractures in rocks, *Tectonophys.* **179**, 345 (1990).

Watanabe, K., Stochastic evaluation of the two-dimensional continuity of fractures in a rock mass, *Int. J. Rock Mech. Min. Sci. Geomech. Abstr.* **23**, 431 (1986).

Witherspoon, P. A., Amick, C. H., Gale, J. E., and Iwai, K., Observations of a potential size effect in experimental determination of the hydraulic properties of fractures, *Water Resour. Res.* **15**, 1142 (1979).